


ARTICLE

An antibody toolbox to track complex I assembly defines AIF's mitochondrial function

Anjaneyulu Murari¹, Shauna-Kay Rhooms¹, Naga Sri Goparaju¹, Maximino Villanueva¹, and Edward Owusu-Ansah^{1,2} 

An ability to comprehensively track the assembly intermediates (AIs) of complex I (CI) biogenesis in *Drosophila* will enable the characterization of the precise mechanism(s) by which various CI regulators modulate CI assembly. Accordingly, we generated 21 novel antibodies to various mitochondrial proteins and used this resource to characterize the mechanism by which apoptosis-inducing factor (AIF) regulates CI biogenesis by tracking the AI profile observed when AIF expression is impaired. We find that when the AIF–Mia40 translocation complex is disrupted, the part of CI that transfers electrons to ubiquinone is synthesized but fails to progress in the CI biosynthetic pathway. This is associated with a reduction in intramitochondrial accumulation of the Mia40 substrate, MIC19. Importantly, knockdown of either MIC19 or MIC60, components of the mitochondrial contact site and cristae organizing system (MICOS), fully recapitulates the AI profile observed when AIF is inhibited. Thus, AIF's effect on CI assembly is principally due to compromised intramitochondrial transport of the MICOS complex.

Introduction

Mitochondrial complex I (CI; NADH: ubiquinone oxidoreductase) is the largest holoenzyme of the oxidative phosphorylation system (OXPHOS). Mammalian CI has 45 subunits, which are assembled through multiple steps. During CI assembly, two or more specific subunits consistently associate with each other to form a specific assembly intermediate (AI). Various independently formed AIs ultimately merge with each other or individual subunits en route to forming the mature holoenzyme. We previously showed that the mechanism of CI assembly in *Drosophila melanogaster* flight (thoracic) muscles is similar to what has been described in mammalian systems, as similar AIs are formed during CI assembly in *Drosophila* and mammalian systems (Garcia et al., 2017; Rhooms et al., 2019). Generating antibodies for a select set of *Drosophila* CI subunits that encompass all known AIs that are formed during CI biogenesis will make it possible to comprehensively track CI AIs via immunoblotting. This will enable the characterization of the precise mechanism(s) by which various CI regulators modulate CI assembly in vivo in *Drosophila* tissues.

Apoptosis-inducing factor (AIF) is a nuclear-encoded oxidoreductase that is largely localized to the intermembrane space of the mitochondrion (Susin et al., 1999; Arnoult et al., 2002; Otera et al., 2005; Yu et al., 2009). When the mitochondrial outer membrane is permeabilized, leading to a collapse of the

mitochondrial membrane potential, a soluble form of AIF is released into the cytosol. This soluble form of AIF translocates to the nucleus to initiate extensive DNA fragmentation and widespread chromatin condensation during apoptosis (Susin et al., 1999; Yu et al., 2002). In addition, AIF moonlights as a regulator of mitochondrial function, although the precise mechanism has not been fully resolved. Mice in which AIF has been depleted from their forebrains display defects in development of the cerebral cortex due to excessive mitochondrial fragmentation and aberrant cristae formation (Cheung et al., 2006). Accordingly, mutations in AIF cause major alterations in the OXPHOS system and are associated with both neurodegeneration and muscle atrophy in multiple model organisms and humans (Klein et al., 2002; Wischhof et al., 2018; Ghezzi et al., 2010; Rinaldi et al., 2012; Ardisson et al., 2015; Berger et al., 2011; Vahsen et al., 2004; Troulinaki et al., 2018).

We sought to define the mechanism(s) by which AIF regulates mitochondrial CI function in *Drosophila* flight muscles. We generated 21 novel antibodies to various mitochondrial proteins (15 of which were raised against CI proteins) and have used classical *Drosophila* genetics and immunoblotting of AIs to characterize the mechanism by which AIF regulates CI biogenesis in vivo. The 21 novel antibodies include seven that were raised against all seven mitochondrial DNA (mtDNA)-encoded

¹Department of Physiology and Cellular Biophysics, Columbia University Medical Center, New York, NY; ²The Robert N. Butler Columbia Aging Center, Columbia University Medical Center, New York, NY.

Correspondence to Edward Owusu-Ansah: eo2364@cumc.columbia.edu.

© 2020 Murari et al. This article is distributed under the terms of an Attribution–Noncommercial–Share Alike–No Mirror Sites license for the first six months after the publication date (see <http://www.rupress.org/terms/>). After six months it is available under a Creative Commons License (Attribution–Noncommercial–Share Alike 4.0 International license, as described at <https://creativecommons.org/licenses/by-nc-sa/4.0/>).

CI subunits, which have been notoriously difficult to generate antibodies for, due to their highly hydrophobic nature. In fact, antibodies targeting all seven mtDNA-encoded CI subunits have not been developed for any organism.

We find that RNAi-mediated inhibition of the *Drosophila* orthologue of AIF produces a CI AI profile that is essentially the same as what is observed when components of the mitochondrial intermembrane space (MIA) disulfide relay-dependent import system are knocked down. AIF disruption arrests the assembly of both nuclear- and mtDNA-encoded CI subunits, such that the part of CI that transfers electrons to ubiquinone (Q module) is synthesized but fails to advance further in the CI biosynthetic pathway. Additionally, AIF disruption impairs the assembly of multiple mtDNA-encoded CI subunits, leading to a stalling in the biogenesis of the membrane domain (P module) of CI. This is associated with a reduction in the amount of the Mia40 substrate MIC19 that accumulates in the mitochondrion. Importantly, RNAi-mediated knockdown of either MIC19 or MIC60 fully recapitulates the AI profile observed when AIF or components of the Mia40 translocation system are genetically disrupted. We conclude that the effect of AIF disruption on CI AI profiles can largely be attributed to a failure to transfer components of the MICOS (mitochondrial contact site and cristae organizing system) complex into the inner mitochondrial membrane. We anticipate that future studies using this novel resource of 21 antibodies will be instrumental in systematically defining the mechanism by which novel candidate regulators of CI assembly regulate CI assembly in vivo.

Results

RNAi-mediated disruption of *Drosophila* AIF in adult flight muscles impairs the assembly of multiple OXPHOS complexes

The *Drosophila* orthologue of AIF is CG7263, hereafter referred to as dAIF. To explore the biochemical consequences of impairing dAIF function in adult flight muscles, we expressed a transgenic RNAi construct of dAIF in flight muscles via the Gal4/upstream activating sequence (UAS) system (Brand and Perrimon, 1993). We used three different Gal4 lines with varied periods and potencies of expression in order to achieve what we refer to as strong (Dmef2-Gal4/UAS-dAIF^{RNAi}), moderate (Ubi-Gal4/UAS-dAIF^{RNAi}), and weak (Mhc-Gal4/UAS-dAIF^{RNAi}) disruption of dAIF in the flight muscles. Henceforth, we refer to these genotypes as dAIF-s, dAIF-m, and dAIF-w flies, respectively. Western blotting with an antibody raised against dAIF confirmed that dAIF was down-regulated, albeit to different extents in flight muscles isolated from the dAIF-s, dAIF-m, and dAIF-w flies (Fig. 1 A).

We assessed the effect of knocking down dAIF expression on the assembly of the OXPHOS complexes in adult flight muscles. We isolated mitochondria from thoraxes of the dAIF-s, dAIF-m, and dAIF-w flies and evaluated the integrity of their OXPHOS complexes using silver staining and blue native PAGE (BN-PAGE). Knocking down dAIF expression disrupted the assembly of multiple OXPHOS complexes, as the assembly of CI, complex III (CIII), complex IV (CIV), and complex V (CV) were all impaired to different extents (Fig. 1, B and C). The

OXPHOS phenotype observed when dAIF function was disrupted correlated with the relative potency of the Gal4 lines used to express the UAS-dAIF^{RNAi} transgene (Fig. 1, B and C). A CRISPR-mediated mutation of dAIF generated specifically in muscles also resulted in the disruption of multiple OXPHOS complexes, confirming our results obtained with the transgenic RNAi construct (Fig. 1 D). In gel CI, CIV, and CV activities were also reduced in the dAIF-knockdown samples and revealed that the assembly of the CI-CIII₂ supercomplex and the CV dimer (CV₂) was impaired as well when dAIF was genetically disrupted (Fig. 1 E).

RNAi-mediated disruption of *Drosophila* AIF in adult flight muscles causes an up-regulation of cytoprotective genes

To explore whether cytoprotective genes are induced in AIF-s or AIF-w muscles as an adaptive compensatory response to disruption of AIF, we analyzed the expression profile of genes known to function as chaperones or implicated in oxidative stress responses within 2 d after the AIF-s and AIF-w flies eclosed as adults. We observed that cytosolic chaperones such as *hsp70* and *hsp26* were more potently induced in the AIF-w samples. However, while the mitochondrial chaperone *hsp22* was robustly up-regulated in both AIF-s and AIF-w samples, it showed a greater induction in AIF-s samples (Fig. 2 A). Interestingly, several genes implicated in oxidative stress responses (glutathione S transferases and peroxiredoxins) showed a trend of more potent induction in the AIF-s samples (Fig. 2 B). Thus, cytoprotective genes are induced in both AIF-s and AIF-w samples, but cytosolic processes are likely to be more preserved in AIF-w flies due to a stronger up-regulation of cytosolic chaperones.

dAIF knockdown suppresses locomotory activity and sensitizes flies to multiple stresses

To evaluate the functional consequences of the biochemical defects and cytoprotective responses observed when dAIF is genetically disrupted, we analyzed the locomotory behavior of dAIF-s, dAIF-m, and dAIF-w flies. The relatively weak knockdown of dAIF-w flies did not produce any readily perceptible climbing defects; however, climbing ability was impaired in the dAIF-m flies, while a severe climbing defect was observed for the dAIF-s flies, with most dAIF-s flies essentially paralyzed (Fig. 3 A). Interestingly, monitoring the spontaneous physical activity of these flies over a 6-d period after eclosure revealed that the dAIF-w flies appeared to be more physically active than wild-type controls. However, the dAIF-m flies were less active than their corresponding wild-type controls, while the dAIF-s flies were essentially disabled in line with observations made with the climbing assay (Fig. 3 B).

Survival curve analyses showed that both dAIF-m and dAIF-s flies ultimately succumb to lethality, with ~50% of the dAIF-m flies surviving to 5 d after eclosure, while lifespan had been extinguished in the dAIF-s population by the aforementioned time point (Fig. 3 C). When fed a sugar diet, which can be metabolized by glycolysis to generate energy, with minimal contribution from the mitochondrion, the dAIF-s flies fared reasonably well, with ~80% surviving after 2 d (Fig. 3 D).

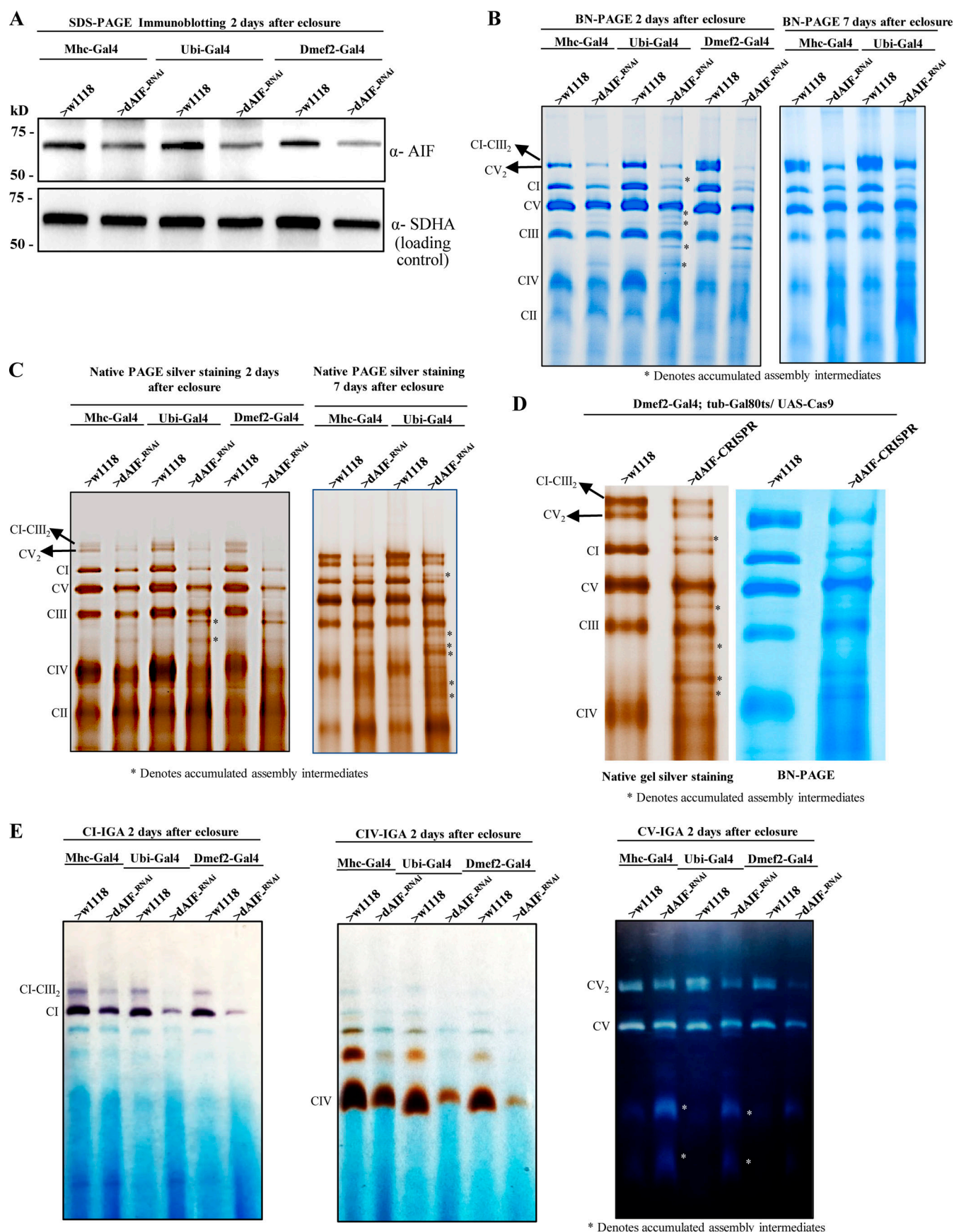


Figure 1. Disruption of *Drosophila* AIF in adult flight muscles impairs the assembly of multiple OXPHOS complexes. (A) SDS-PAGE and immunoblotting of total cell lysates from flight muscles isolated from adult flies with the genotypes shown. (B) BN-PAGE of mitochondrial preparations from flight muscles of flies with the genotypes shown. dAIF-s flies do not survive to 7 d after eclosion. (C) BN-PAGE and silver staining of the mitochondrial preparations in B. (D) Silver staining and BN-PAGE analyses of mitochondrial preparations from flight muscles expressing a CRISPR construct targeting dAIF. (E) CI (left panel), CIV (middle panel), and CV (right panel) in gel activity of OXPHOS complexes isolated from flight muscles of flies with the genotypes shown. CII, complex II.

However, ~25% of dAIF-s flies (compared with 75% in wild-type controls) survived when starved for 48 h (Fig. 3 D). This is likely because starvation requires the mobilization of lipid stores for the generation of ATP by the mitochondrion and because the relatively unhealthy mitochondria in dAIF-s flies were incompatible with survival under these circumstances. In line with this thought, the dAIF-s population failed to survive to the 48-h mark when fed a high-fat diet that requires functional mitochondria to metabolize. This contrasts with the fact that ~40% of wild-type flies survived this dietary regimen (Fig. 3 D).

A comparison of the biochemical, gene expression, and functional data indicated that the mitochondrial dysfunction phenotype of the dAIF-s flies most likely represents a terminal phenotype, where it will be difficult to distinguish primary from secondary consequences of dAIF disruption. Accordingly, we pursued our additional studies exploring the molecular mechanism by which AIF regulates CI assembly largely with the dAIF-m and dAIF-w flies.

The biogenesis of several AIs-containing nuclear-encoded subunits are stalled when dAIF is disrupted

To gain additional insights into the mechanism by which dAIF regulates OXPHOS assembly, we analyzed the effect of disrupting dAIF on CI AIs. Mammalian CI has 45 subunits (44 distinct subunits, one of which appears twice in the complex) that

are assembled via a highly regulated process to form a boot-shaped structure consisting of a matrix and membrane domain (Fiedorczuk et al., 2016; Agip et al., 2018; Fig. 4 A). CI biogenesis proceeds through multiple steps and involves a number of independently formed AIs that merge with each other or other subunits en route to forming the mature complex (reviewed in Formosa et al., 2018; Figs. 4 B and S1 A). The AIs correspond to partial or complete domains of the three functional modules of CI. The NADH dehydrogenase module (N module), which is located at the tip of the matrix domain, is the site of NADH oxidation. Situated between the N module and the membrane domain is the Q module, which is responsible for ubiquinone reduction. The membrane domain consists of the proton-conducting P module and can be subdivided into a proximal P_P module and distal P_D module (Fig. 4 A). We used a commercially available antibody (anti-NDUFS3) that detects dNDUFS3 to track the integrity of AIs containing the Q module by Western blotting of blue native gels. AIs containing the N, P_P, and P_D modules were tracked primarily by immunoblotting with antibodies we raised against anti-dNDUFV1, anti-dNDUFS5, and anti-dNDUFB5, respectively. In some instances, an antibody we generated against dNDUFB6 was also used to detect the P_D module to confirm results obtained with the anti-dNDUFB5 antibody (Figs. 4 A and S1 A).

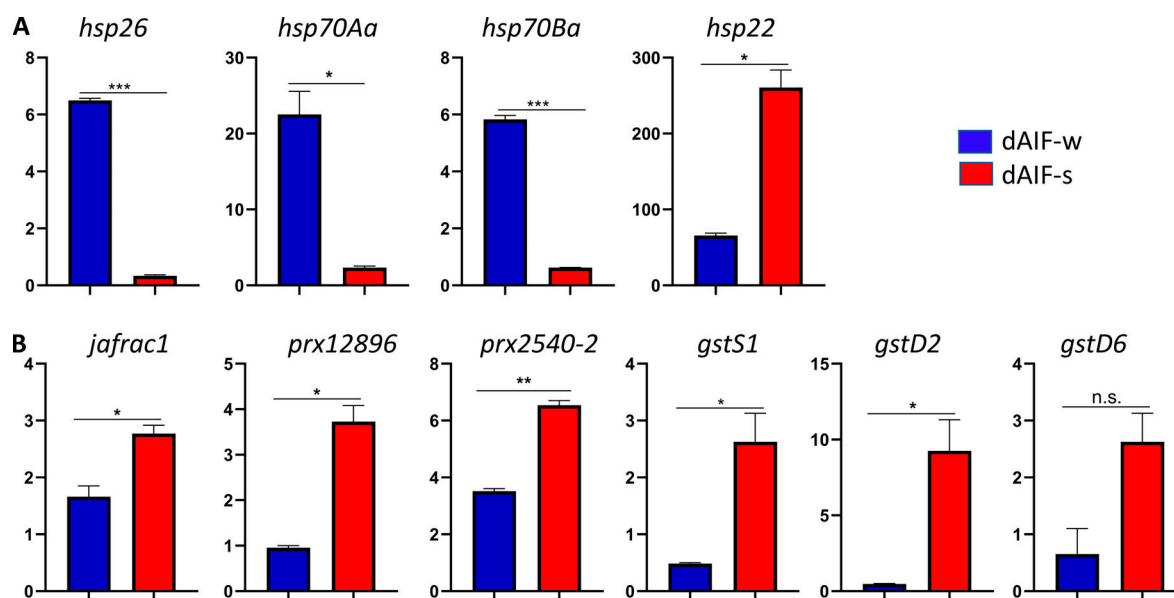


Figure 2. RNAi-mediated disruption of *Drosophila* AIF in adult flight muscles causes an up-regulation of cytoprotective genes. (A) Relative transcript levels of the heat shock proteins shown in dAIF-w and dAIF-s flies relative to wild-type controls 2 d after eclosion. (B) Relative transcript levels of *Jafracl* (CG1633), a peroxiredoxin referred to here as *Prx12896* (CG12896), *Prx2540-2* (CG11765), *GstS1* (CG8938), *GstD2* (CG4181), and *GstD6* (CG4423) in dAIF-w and dAIF-s flies relative to wild-type controls 2 d after eclosion. In all instances, three biological replicates with 10 flies per replicate were used, and P values are based on the Student's *t* test for unpaired two-tailed samples. The fold change shown refers to the mean \pm SD. n.s., $P > 0.05$; *, $P < 0.05$; **, $P < 0.01$; ***, $P < 0.001$.

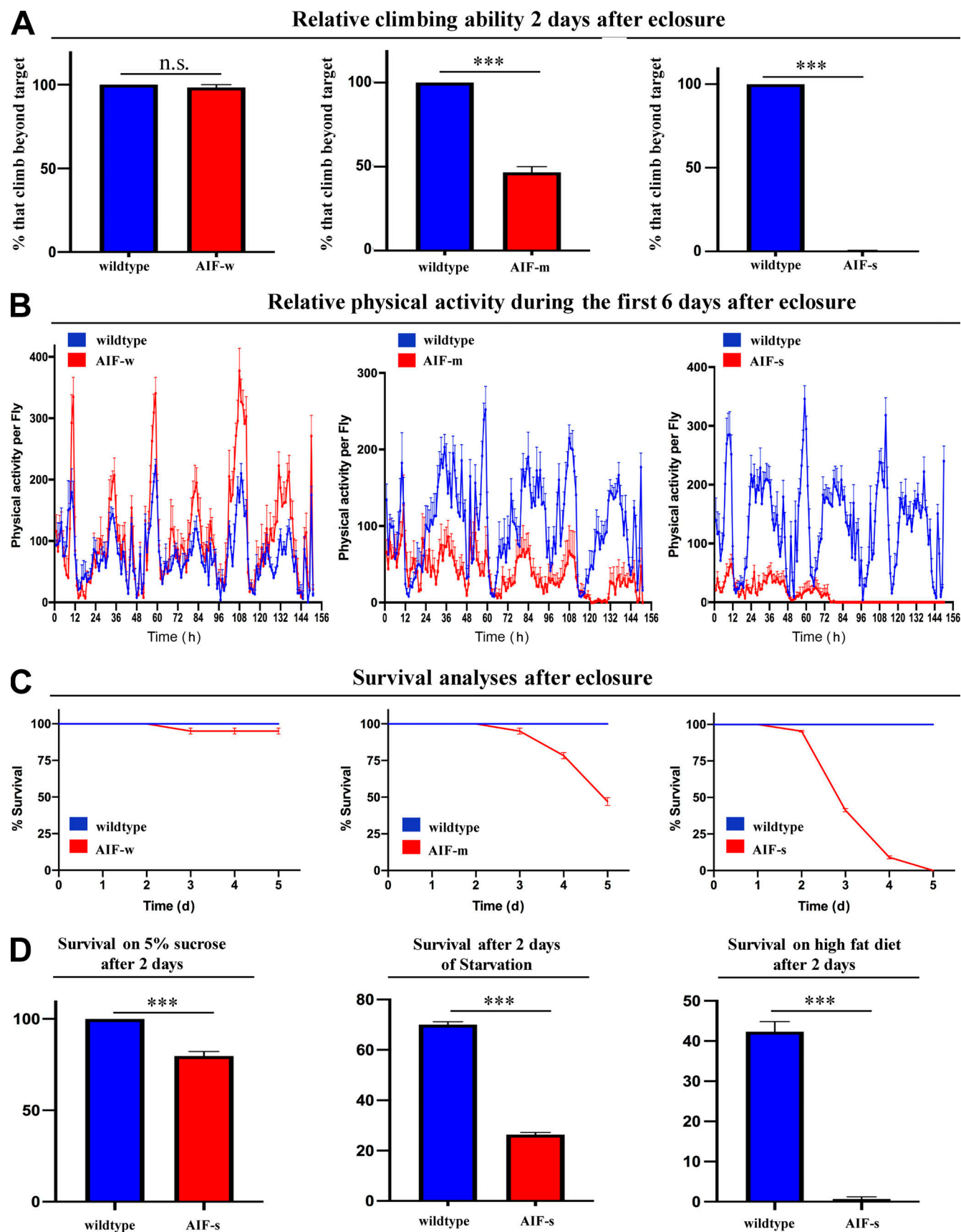


Figure 3. **dAIF knockdown suppresses locomotory activity and sensitizes flies to multiple stresses.** (A) Relative climbing ability of dAIF-w, dAIF-m, and dAIF-s flies relative to wild-type controls. (B and C) Spontaneous physical activities (B) and survival curves (C) of dAIF-w, dAIF-m, and dAIF-s flies. (D) Survival of dAIF-s flies relative to wild-type controls when raised on the diets shown. $n = 3$ biological replicates with 100 flies per replicate; P values are based on the Student's *t* test for unpaired two-tailed samples. The fold change shown refers to the mean \pm SEM. n.s., $P > 0.05$; ***, $P < 0.001$.

We first tracked the incorporation of dNDUFS5 (CG11455) into the P_P module in mitochondria isolated from the flight muscles of dAIF-m and dAIF-w flies. RNAi-mediated knockdown of dAIF resulted in a reduction in the amount of dNDUFS5 that had incorporated into the P_P module, such that the amounts of the Q+P_P and Q+P AIs that had formed were reduced relative to wild type (Fig. 4 C). Notably, the impairment of CI assembly at the level of the Q+P_P module caused a significant backlog of the Q module, as assessed by anti-NDUFS3 immunoblotting (Figs. 4 D and S1 B). Disruption of dAIF caused a significant accumulation of AIs containing the P_D module as well, most likely because the dysfunctional Q+P_P module could not bind to the independently formed P_D module for CI assembly to proceed (Fig. 4, E and F). Knocking down dAIF also led to a reduction in the amount of dNDUFV1 that had incorporated into the N module (Fig. S1 C). Accordingly, dAIF disruption impairs the biogenesis of the P_P module and causes a stalling of other CI AIs.

We note that the effect of dAIF disruption on the integrity of AIs was not limited to CI, as CV AIs also accumulated in response to dAIF disruption, as assessed by anti-ATP-SynBeta immunoblotting (Fig. 4 G). We raised antibodies against additional CI subunits such as dNDUFS2, dNDUFS6, dNDUFA12, and dNDUFB8 to examine the steady-state levels of multiple CI proteins. We found that unincorporated subunits that would have been assembled into any of the CI AIs were ultimately degraded, as SDS-PAGE Western blot analyses revealed that the total residual amounts of all CI subunits tested were reduced in dAIF-s, dAIF-m, and dAIF-w samples (Fig. 4 H). Similarly, using the anti-ATP-SynBeta antibody and antibodies we generated to detect dUQCRC2, dCOXIV, and dmtCOXII revealed that the amounts of dUQCRC2 (CIII), dCOXIV (CIV), dmtCOXII (CIV), and dATP-SynB were reduced in samples expressing RNAi to dAIF (Fig. 4 I). Although the most robust effects of dAIF disruption were on CI and CIV, dAIF regulates the assembly of the whole OXPHOS complex. However, for the rest of this manuscript we have focused our attention primarily on the mechanism by which dAIF regulates CI assembly.

dAIF is required for the assembly of mtDNA-encoded subunits

7 of the 44 distinct CI subunits are encoded by mtDNA. The seven mtDNA-encoded subunits are dND1, dND2, dND3, dND4, dND4L, dND5, and dND6 and are part of the P module. Specifically, dND1, dND2, dND3, dND4L, and dND6 are part of the P_P module, while dND4 and dND5 are part of the P_D module (reviewed in Formosa et al., 2018). We explored whether dAIF disruption impairs the incorporation of mtDNA-encoded CI subunits into the membrane domain (Fig. 4 A).

To this end, we raised antibodies against all seven mtDNA-encoded CI subunits to examine their expression via SDS-PAGE immunoblotting. We found that the level of expression of the mtDNA-encoded CI subunits in flight muscles expressing transgenic RNAi constructs to various mitochondrial ribosomal proteins was impaired, confirming their dependence on mitochondrial translation (Fig. 5 A). Interestingly, the extent to which the expression of each mtDNA-encoded CI subunit was diminished varied with the different mitochondrial ribosomal

protein transgenic RNAi flies. However, a consistent pattern emerged; the pore-forming subunits (i.e., dND2, dND4, and dND5) appeared to be more stable than the other mtDNA-encoded CI subunits, as their expression varied only marginally when mRpS16 was knocked down (Fig. 5 A). Indeed, due to the extreme stability of dND2 and dND4, RNAi-mediated knockdown of either mRpS21 or mRpS29 did not markedly reduce the expression of dND2 and dND4. However, we note that even the mitochondrial ribosomal proteins that had the weakest effects on dND2 and dND4 when disrupted caused potent reductions in dND3, dND4L, and dND6 expression (Fig. 5 A). Similarly, when the expression of dAIF was knocked down, the amounts of dND3, dND4L, and dND6 were reduced, irrespective of whether a weaker or stronger Gal4 driver was used (Fig. 5 B). However, readily noticeable reductions in ND1, ND2, and ND5 were only observed when the strongest Gal4 driver (Dmef2-Gal4) was used to knock down dAIF expression (Fig. 5 B). These results indicate that dND3, dND4L, and dND6 have relatively short half-lives when compared with the other mtDNA-encoded CI subunits. This observation is pivotal to how we interpret the phenotypes with the mtDNA-encoded CI subunits. We deduce from these results that when mitochondrial translation is inhibited, the expression of dND3, dND4L, and dND6 will likely be depleted before the other dND subunits. The depletion and consequent failure to incorporate dND3, dND4L, and dND6 into AIs may initially manifest as a backlog of some of the other more stable mtDNA-encoded CI subunits, even though mitochondrial translation is inhibited.

Accordingly, disruption of dAIF caused a stalling and accumulation of smaller AIs containing dND1, dND4, and dND5. However, the amount of dND2, dND3, dND4L, and dND6 present in AIs was reduced in both dAIF-m and dAIF-w samples (Fig. 5, C–I; and Fig. S2). The reduced expression of dND2, dND3, dND4L, and dND6 in dAIF-w samples 2 d after eclosure is unlikely to be a secondary consequence of a failure to incorporate dNDUFS5 into the P_P module. If that were the case, the uninterrupted biogenesis of all mtDNA-encoded CI subunits would have led to an accumulation of all mtDNA-encoded CI subunits instead. Taken together, these results indicate that dAIF disruption impairs the assembly of mtDNA-encoded subunits independent of its effect on nuclear-encoded CI subunits.

Disruption of dMia40 and dErv1 produces a CI AI profile that is similar to what is observed when dAIF is disrupted

AIF is a component of the MIA disulfide relay-dependent import pathway (Meyer et al., 2015; Hangen et al., 2015; Modjtahedi and Kroemer, 2016). Other primary components of this pathway are the oxidoreductase Mia40/CHCHD4 and the sulfhydryl oxidase Erv1/ALR (Hell, 2008). *Drosophila* orthologues of Mia40 and Erv1 are CG7950 and CG12534, respectively, henceforth referred to as dMia40 and dErv1. Interestingly, we knocked down the expression of dMia40 and dErv1 and observed that the assembly of multiple OXPHOS complexes was impaired (Fig. 6 A), similar to results obtained when dAIF was knocked down (Fig. 1, B, C, and E). To delve into the extent to which the AI phenotypes observed in flight muscles isolated from the dAIF-m and dAIF-w flies are

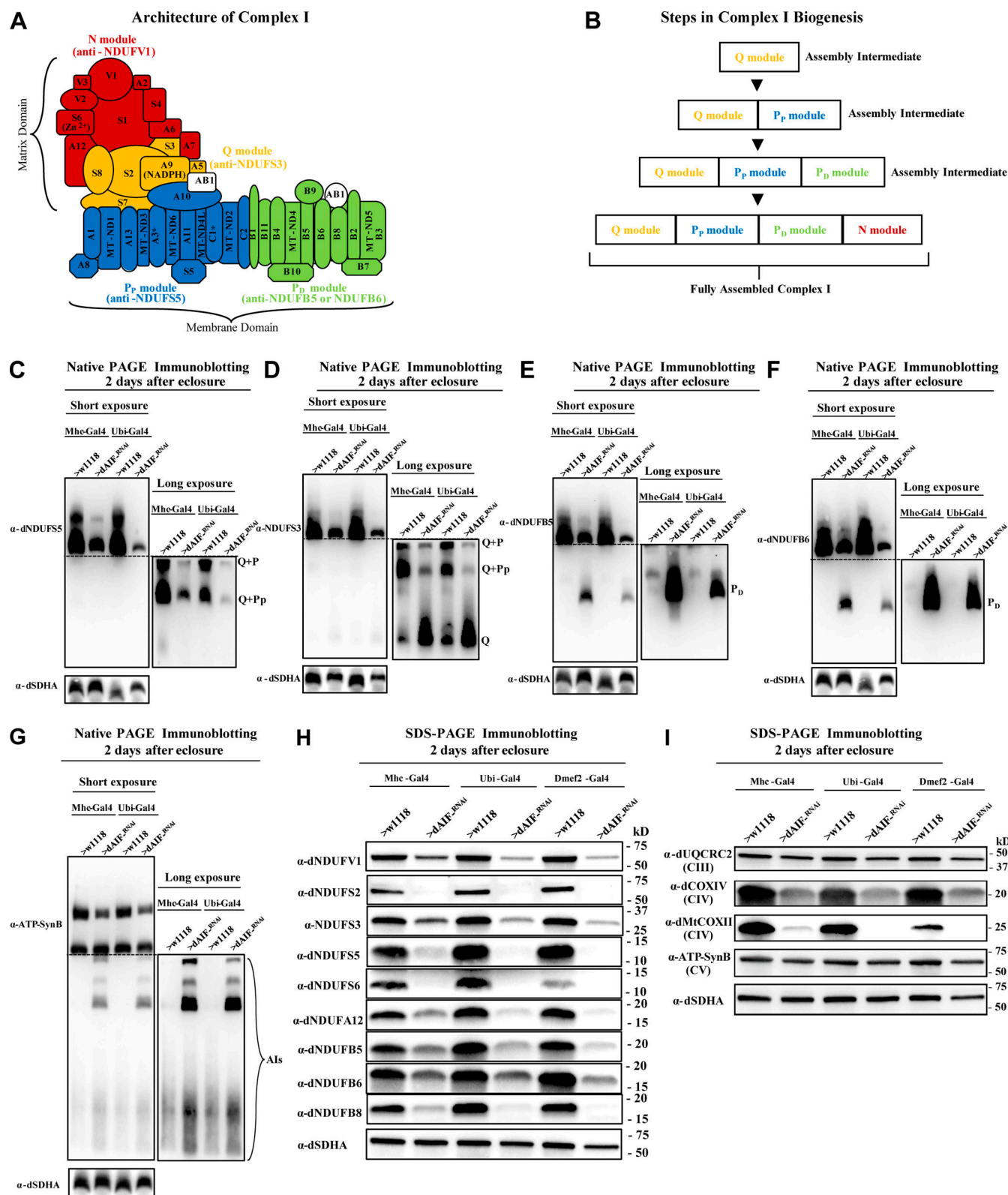
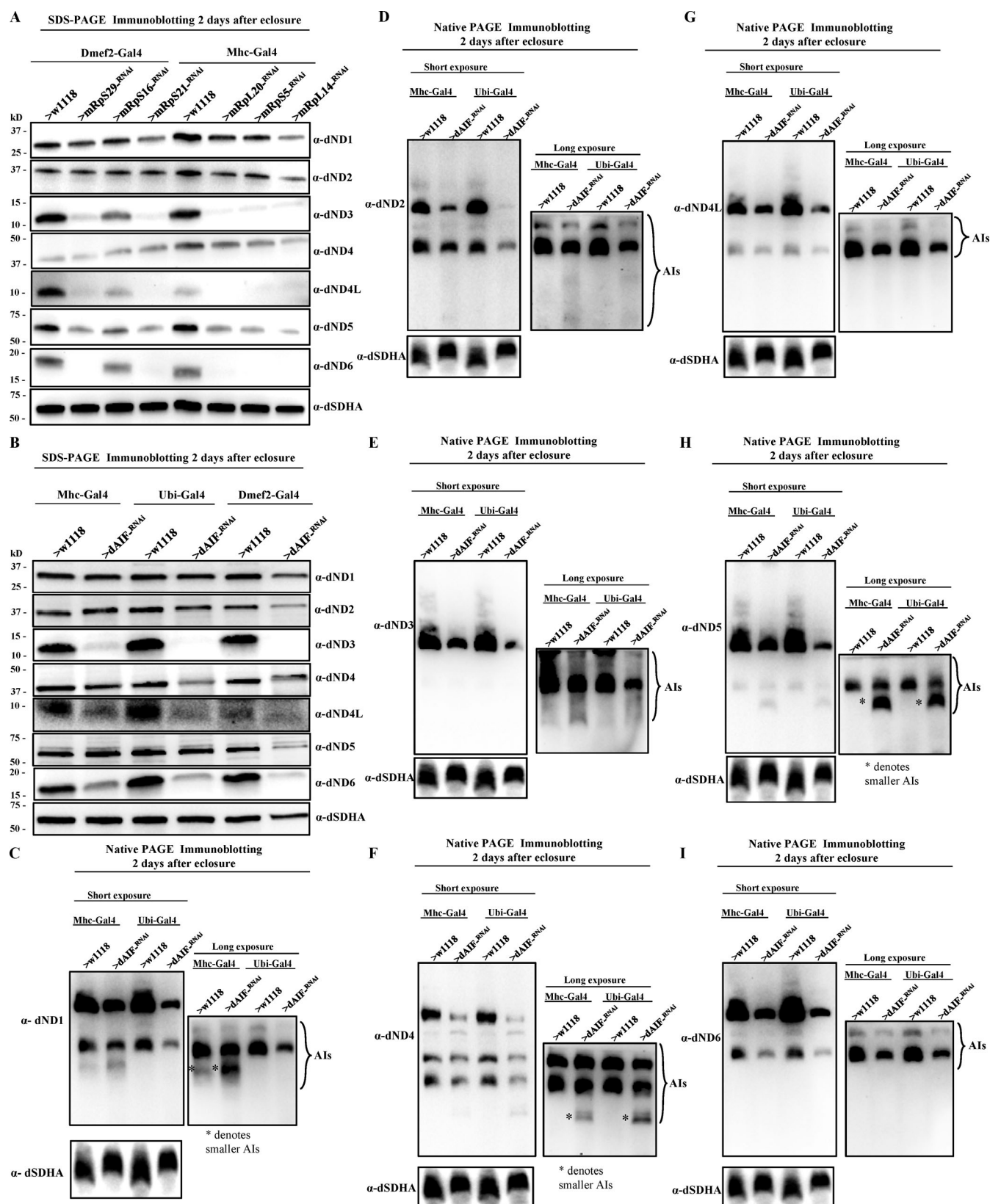


Figure 4. The biogenesis of several AIs containing nuclear-encoded subunits is stalled when dAIF is disrupted. (A) A representation of mammalian CI showing the approximate relative positions of the 45 subunits. The first four letters of the nuclear-encoded subunit names have been eliminated for simplicity. The N, Q, P_p, and P_d modules are color-coded in red, orange, blue, and green, respectively. The antibodies used to track the various modules are shown and color-coded accordingly. (B) A schematic depicting the step-wise assembly process of CI. AIs corresponding to the Q, P_p, Q+P_p, and Q+P_p+P_d (i.e., Q+P) modules can be tracked by immunoblotting. (C–G) Mitochondrial preparations from flight muscles isolated from adult flies with the genotypes shown were analyzed by BN-PAGE, followed by immunoblotting with the indicated antibodies. (H and I) Total cell lysates from flight muscles isolated from adult flies with the genotypes shown were analyzed by SDS-PAGE and immunoblotting with the CI antibodies indicated (H) and the CIII, CIV, and CV antibodies indicated (I).



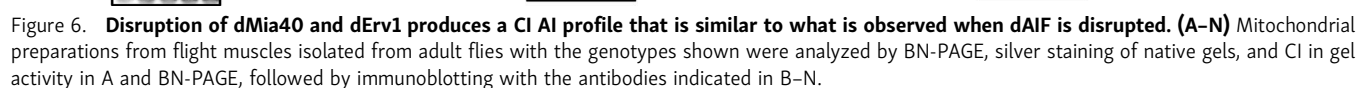
dependent on the disulfide relay-dependent import machinery, we knocked down the expression of dMia40 and dErv1 and examined the distribution of AIs formed. RNAi-mediated disruption of either dMia40 or dErv1 decreased the amount of dNDUFS5 that had incorporated into the P_P module (Fig. 6 B). In remarkable similarity to results obtained when the expression of dAIF is knocked down, a reduction in the amount of dNDUFS5 in the P_P module was associated with a significant backlog in the Q and P_D modules (Fig. 6, C and D). The assembly of the mtDNA-encoded subunits was impeded as well, as there was a decline in the amount of dND3, dND4L, and dND6 present in AIs (Fig. 6, E–G). In addition, there was some accretion of smaller AIs containing dND2 and dND5 (Fig. 6, H and I).

There are at least four CI subunits that are putative substrates for translocation into the mitochondrion via the dMia40 pathway. They are dNDUFA8, dNDUFS5, dNDUFB7, and dNDUFB10 (Hangen et al., 2015; Formosa et al., 2018). We explored whether RNAi-mediated disruption of any of the putative CI dMia40 substrates can reproduce the full range of AI phenotypes observed when dAIF, dMia40, or dErv1 is disrupted. We reasoned that such an experiment will help resolve whether the CI AI profile observed when dAIF, dMia40, or dErv1 is genetically disrupted is due largely to the compromised translocation of one of the CI dMia40 substrates. Consequently, we expressed transgenic RNAi constructs to dNDUFA8, dNDUFS5, dNDUFB7, and dNDUFB10 specifically in flight muscles and analyzed their CI AI profiles. When dAIF, dMia40, or dErv1 is genetically disrupted, the Q module stalls and accumulates, but larger AIs containing the Q module (such as the Q+P_P and the Q+P modules) are reduced relative to wild-type cells (Figs. 4 D and 6 C). However, of the four putative CI dMia40 substrates, it was only the disruption of dNDUFA8 that caused a stalling and accumulation of the Q module, and in fact disruption of all four putative dMia40 substrates actually caused a stalling and accumulation of larger AIs containing the Q module, in stark contrast to what is observed when dAIF, dMia40, or dErv1 expression is impaired (Figs. 4 D and 6, C and J). In samples where dAIF, dMia40, or dErv1 expression is knocked down, anti-dNDUFB5 immunoblotting revealed that there is a robust accumulation of an AI containing dNDUFB5, which previous studies have shown corresponds to the P_D module (Garcia et al., 2017; Figs. 4 E and 6 D). However, disruption of dNDUFB7 or dNDUFB10 did not cause robust accumulation of the P_D module (Fig. 6 K). Importantly, AIs containing dND3, dND4L, or dND6 were not reduced when any of the putative dMia40 substrates were genetically disrupted, and in fact in some instances, their expression increased (Fig. 6, L–N). The reduced expression of AIs containing mtDNA-encoded CI subunits such as dND3, dND4L, or dND6 is a cardinal phenotype observed when dAIF, dMia40, or dErv1 expression is knocked down (Fig. 5, E, G, and I; and Fig. 6, E–G). Because RNAi-mediated knockdown of none of the putative CI dMia40 substrates completely recapitulates the CI AI phenotypes observed when dAIF, dMia40, or dErv1 is disrupted, we conclude that the AI phenotype observed when dAIF, dMia40, or dErv1 expression is disrupted is not due to the compromised translocation of any one dMia40 CI substrate into the mitochondrion.

Impairing the production of the Q, N, or P_P modules does not inevitably lead to a reduction in expression of dND3, dND4L, and dND6

The block in assembly of the mtDNA-encoded subunits could be a secondary effect, emanating from the impaired import of all the CI subunits that are imported via the dMia40- and dErv1-mediated disulfide relay system. Alternatively, dAIF could independently actively regulate the biogenesis and/or incorporation of the mtDNA-encoded subunits into various AIs. We reasoned that if the arrested assembly of mtDNA-encoded subunits precedes the diminished integration of dNDUFS5 into the P_P module, this will be clear evidence that the obstruction in assembly of mtDNA-encoded subunits is not triggered by the impaired import of dNDUFS5. Conversely, if it is the impaired import of CI subunits that are transported via the disulfide relay system that precipitates the arrest in assembly of the mtDNA-encoded subunits, the reduction in the amount of dNDUFS5 in the P_P module will have to occur before the arrest in assembly of the mtDNA-encoded subunits, although additional experiments will be required to definitively prove causality.

To begin to distinguish between these two possibilities, we examined the time of onset of arrest in assembly of the mtDNA-encoded subunits. We used the Gal4/UAS system in combination with the tub-Gal80^{ts} system to knock down the expression of dAIF, dMia40, and dErv1 in flight muscles, commencing after the flies eclosed as adults. In the tub-Gal80^{ts} system, a temperature-sensitive version of Gal80, which is active at 18°C but relatively inactive at 27°C, is expressed ubiquitously by a tubulin promoter (McGuire, Mao and Davis, 2004). Gal80 inhibits Gal4 activity. Therefore, embryos with the genotype Dmef2-Gal4; tub-Gal80^{ts}/UAS-RNAi were raised at 18°C (to prevent Gal4 activity) until they eclosed as adults. Subsequently, the flies were shifted to 27°C for 2, 4, or 6 d to allow the RNAi constructs to be expressed as a result of the relief of Gal4 inhibition by the temperature-sensitive Gal80 (Fig. S3 A). Among the three proteins knocked down, dErv1 appeared to have the shortest half-life, as an AI accumulated in silver-stained native gels by the 2-d time point, which became more prominent after 4 d (Fig. S3 B). In line with these observations, the amount of dNDUFS5 that had been incorporated into the Q+P_P AI by the 2-d time point was reduced when dErv1 was knocked down (Fig. 7 A). This was accompanied by a stalling and accumulation of the Q module, as measured by anti-dNDUFS3 immunoblotting (Fig. 7 B). On the other hand, the expression of dND3 and dND6 was only mildly reduced, if at all, by the 2-d time point. However, a more robust diminution in expression of both dND3 and dND6 was observed at the 4-d time point (Fig. 7, C and D). Similar results were obtained 6 d after the shift to 27°C (Fig. S3, C–F). These data show that while the accumulation of the Q module appears to occur concurrently with the decreased incorporation of dNDUFS5 into the P_P module, the decline in expression of dND3 and dND6 appears to lag behind the interruption in production of the P_P module. The kinetics of appearance of the AI phenotypes did not rule out the possibility that the block in assembly of the mtDNA-encoded subunits may be caused by the decreased incorporation of dNDUFS5 into the P_P module.



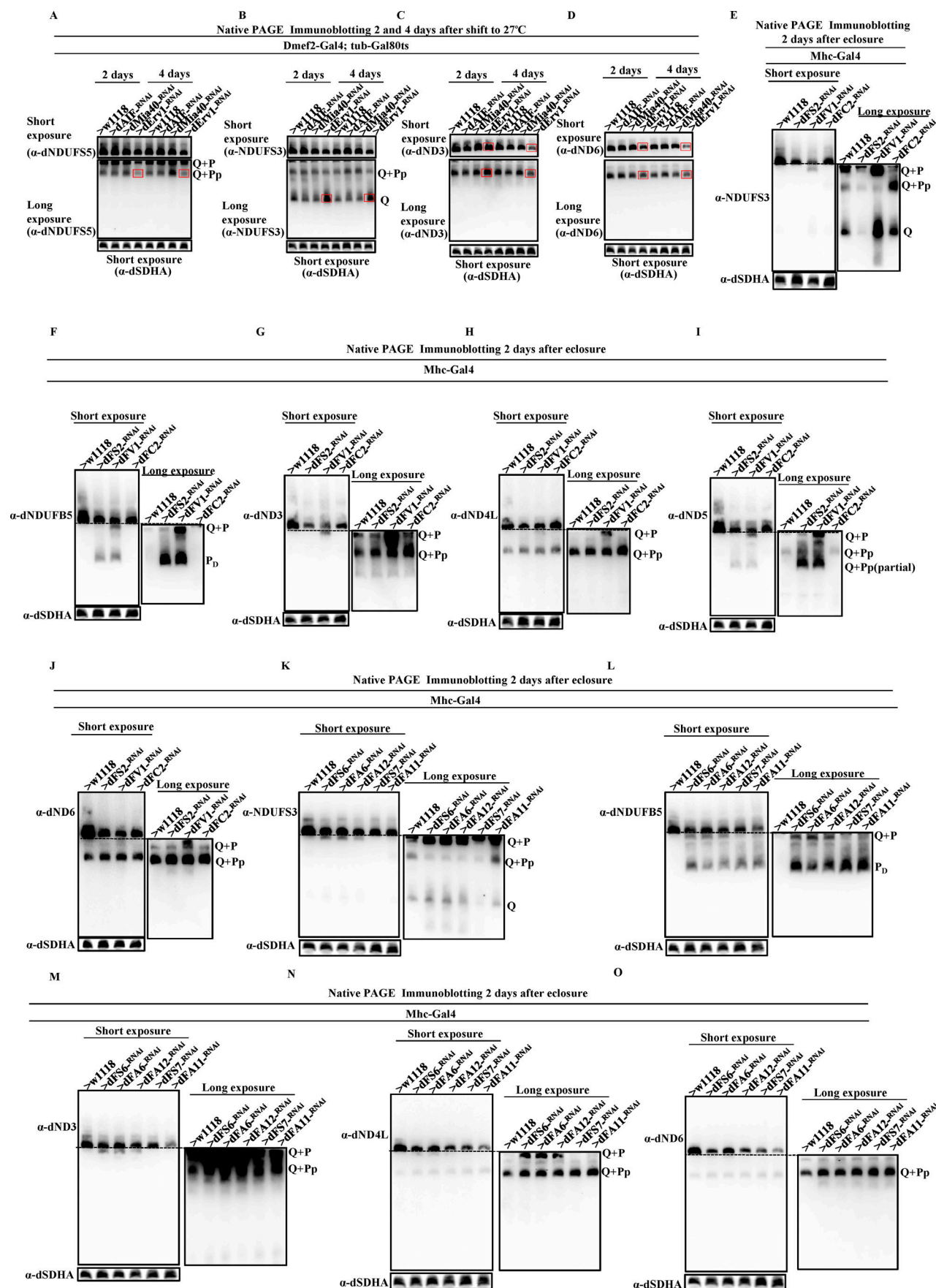


Figure 7. Impairing the production of the Q, N, or P_P modules does not inevitably lead to a reduction in expression of dND3 and dND6. (A–D) All flies express the tub-Gal80^{ts} transgene, where a temperature-sensitive version of Gal80, which is active at 18°C but inactive at 27°C, is expressed ubiquitously by a tubulin promoter. Gal80 inhibits Gal4 activity. Accordingly, embryos expressing Dmef2-Gal4, tub-Gal80^{ts}, and the indicated UAS-RNAi transgenes were raised at 18°C (to prevent Gal4 activity) until they eclosed as adults. Subsequently, the flies were shifted to 27°C for 2 or 4 d to allow the RNAi constructs to be expressed as a result of the relief of Gal4 inhibition by Gal80. Mitochondrial preparations from flight muscles isolated from adult flies with the genotypes shown, 2 or 4 d after shifting to 27°C, were analyzed by BN-PAGE, followed by immunoblotting with the antibodies indicated. The blots were imaged following a short exposure to detect the holoenzyme and supercomplexes, after which the region corresponding to the holoenzyme and supercomplexes was cut off and the rest of the blot reimaged after a long exposure to detect the AIs. The antibodies used were anti-dNDUFS5 (A), anti-NDUFS3, which detects dNDUFS3 (B), anti-dND3 (C), and anti-dND6 (D). Anti-dSDHA was used as a loading control. The lanes showing relevant phenotypes are demarcated in red. **(E–O)** Mitochondrial preparations from flight muscles isolated from adult flies with the genotypes shown were analyzed by BN-PAGE, followed by immunoblotting with the antibodies indicated in the figure.

We used an additional approach to probe whether the thwarted assembly of the mtDNA-encoded subunits is the result of a defective P_P module. A key feature observed during the block in assembly of the mtDNA-encoded subunits is that the amount of AIs containing dND3, dND4L, and dND6 was reduced. If this is simply the passive result of a stalling or disintegration of the P_P, Q, or N modules that happens when dAIF is genetically disrupted, it will be expected that RNAi-mediated disruption of CI subunits that are part of the P_P, Q, or N modules will lead to a similar reduction in the amounts of dND3, dND4L, and dND6 present in AIs. To test this hypothesis, we knocked down the expression of dNDUFS2, dNDUFV1, and dNDUFC2 that are part of the Q, N, and P_P modules, respectively (Fig. 4 A), and analyzed their AI profiles. Disruption of dNDUFS2 abrogated the production of the Q module, while disruption of dNDUFV1 and dNDUFC2 caused a stalling and accumulation of the Q module, most likely due to their effect on disrupting the N and P_P modules, respectively, that would have eventually merged with AIs containing the Q module (Fig. 7 E). Importantly, RNAi-mediated knockdown of dNDUFV1 and dNDUFS2 culminated in a stalling and logjam of the P_D module in line with what happens when the expression of dAIF, dMia40, or dErv1 is knocked down (Figs. 7 F and S4 A). However, there was no decrease in the amounts of dND2, dND3, dND4L, dND5, and dND6 present in AIs when any of dNDUFS2, dNDUFV1, and dNDUFC2 were knocked down (Fig. S4 B and Fig. 7, G–J). Indeed, the level of expression of dND3 appeared to be elevated as a result of disruption of dNDUFV1 and dNDUFC2 (Fig. 7 G). We repeated this experiment with an additional set of five CI subunits (i.e., dNDUFS6, dNDUFA6, dNDUFS7, dNDUFA11, and dNDUFA12). dNDUFS6, dNDUFA6, and dNDUFA12 are part of the N module, while dNDUFS7 and dNDUFA11 are part of the Q and P_P modules, respectively. RNAi-mediated knockdown of these five CI subunits altered the biogenesis or stability of AIs containing the Q module, consistent with their established roles in CI assembly (Garcia et al., 2017; Guerrero-Castillo et al., 2017; Stroud et al., 2016; Fig. 7 K). We found that in all instances, although knocking down the CI subunits gave rise to a stalling of the P_D module as measured by anti-dNDUFB5 and anti-dNDUFB6 immunoblotting, it did not cause a reduction in AIs containing dND3, dND4L, or dND6 (Fig. S4 C and Fig. 7, L–O). In fact, the amounts of dND3, dND4L, or dND6 in AIs either increased or stayed about the same as that in wild-type samples (Fig. 7, M–O). We conclude that a disruption in production of the Q, N, or P_P modules does not necessarily lead to a reduction in

expression of dND3, dND4L, and dND6 and that the observed decrease in expression of dND3, dND4L, or dND6 in AIs when dAIF is knocked down cannot be attributed to dysfunctional Q, N, or P_P modules.

dAIF regulates intramitochondrial localization of the *Drosophila* orthologue of CHCHD3/MIC19

We hypothesized that a Mia40 substrate with a more global effect on mitochondrial function may be responsible for regulating both the nuclear- and mtDNA-encoded phenotypes observed when the AIF–Mia40 translocation system is disrupted. MIC19 is an inner membrane-bound protein that is part of the MICOS complex and is known to be a Mia40 substrate (Sakowska et al., 2015; Darshi et al., 2012). We obtained a highly enriched mitochondrial fraction from flight muscles and showed via immunoblotting using an antibody we raised against dMIC19 that RNAi-mediated knockdown of the *Drosophila* orthologue of MIC19 (CG1715, henceforth referred to as dMIC19) essentially abrogates the intramitochondrial accumulation of dMIC19 (Fig. 8, A and B). The amount of dMIC19 that accumulated in mitochondria from thoraxes isolated from dAIF-s, dAIF-m, and dAIF-w flies was reduced, although there was an increased expression of the nuclear-encoded mitochondrial chaperone Hsp60 (Fig. 8 C). Thus, the reduced intramitochondrial accumulation of dMIC19 is not due to a global impairment of mitochondrial import pathways. A similar result was observed when dErv1 was knocked down (Fig. 8 D). Overall, these results are consistent with previous findings showing that MIC19 is a substrate of the AIF–Mia40–Erv1 intramitochondrial translocation system (Sakowska et al., 2015; Darshi et al., 2012).

Disruption of the MICOS complex impairs the biogenesis of AIs containing both nuclear- and mtDNA-encoded CI subunits

We examined the effect of disrupting the MICOS complex on the CI AI profile. RNAi-mediated knockdown of dMIC19 or another MICOS protein, MIC60 (CG6455, henceforth referred to as dMIC60), led to a stalling and accumulation of the Q module as assessed by anti-NDUFS3 immunoblotting (Fig. 9 A). This was associated with a reduction in the amount of dNDUFS5 that had incorporated into the P_P module (Fig. 9 B). In remarkable similarity to results obtained when the expression of components of the AIF–Mia40 translocation system are knocked down, a reduction in the amount of dNDUFS5 in the P_P module occurred concurrently with a substantial backlog of the P_D module (Fig. 9 C). Significantly, the assembly of the mtDNA-encoded CI

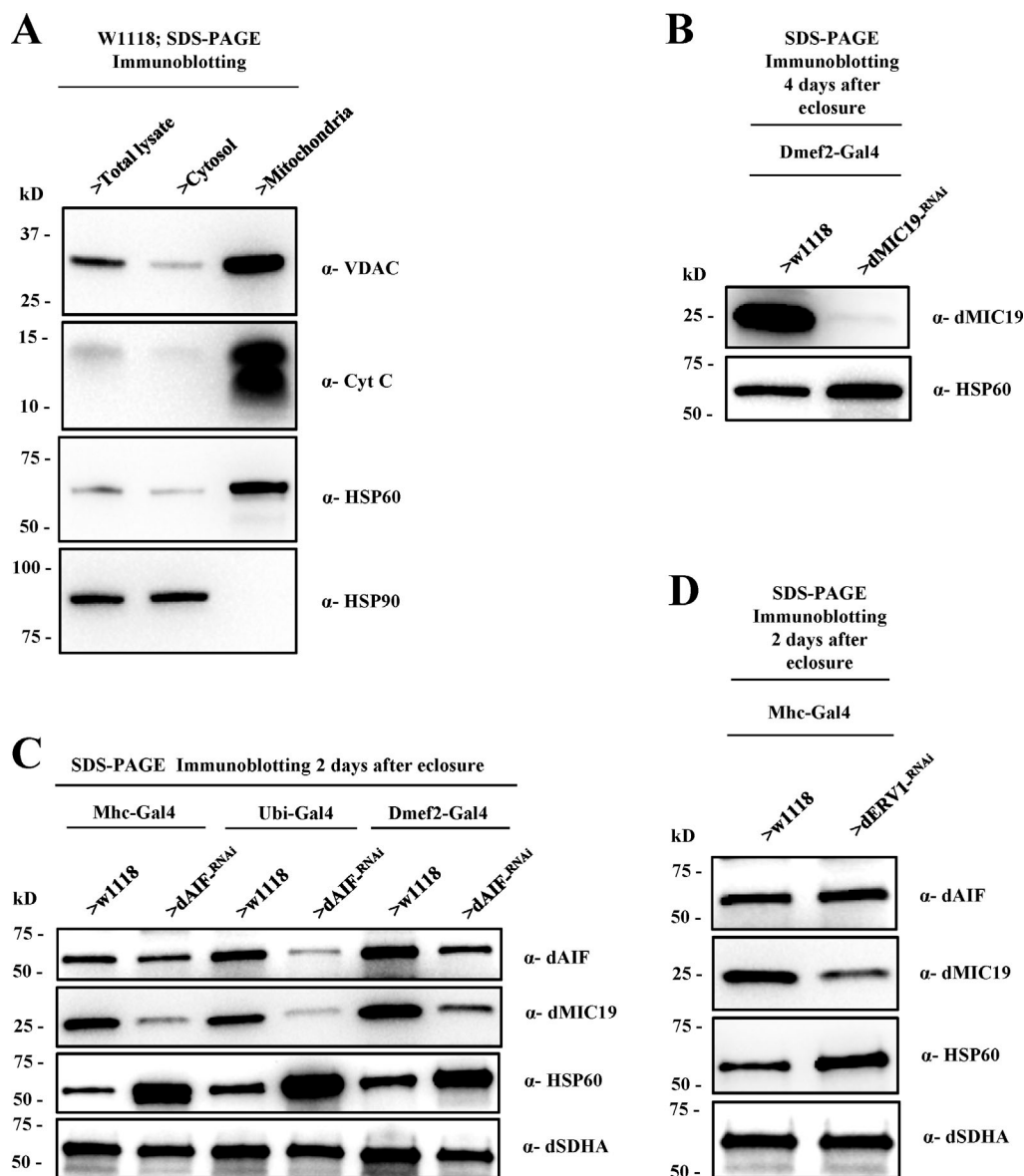


Figure 8. **dAIF regulates intramitochondrial localization of the *Drosophila* orthologue of CHCHD3/MIC19.** (A) A total cell lysate, cytosolic, and mitochondrial-enriched fractions from flight muscles isolated from wild-type (w1118) adult flies were analyzed by SDS-PAGE and immunoblotting with anti-VDAC, anti-CytC, anti-Hsp60, and anti-Hsp90 antibodies to assess mitochondrial purity. The doublet for cytochrome C denotes both the oxidized and reduced forms of the coenzyme. (B) Mitochondrial preparations from flight muscles isolated from wild-type and Dmef2-Gal4/UAS-dMIC19^{-RNAi} flies 4 d after eclosure were analyzed by SDS-PAGE and immunoblotting. RNAi-mediated disruption of dMIC19 significantly reduces the amount of MIC19 that localizes to the mitochondrion. (C) SDS-PAGE and immunoblotting of mitochondrial preparations from flight muscles isolated from adult flies with the genotypes shown 2 d after eclosure. Intramitochondrial accumulation of MIC19 is reduced in all instances where AIF expression is knocked down. (D) SDS-PAGE and immunoblotting of mitochondrial preparations from wild-type and Mhc-Gal4/UAS-dErv1^{-RNAi} flies 2 d after eclosure. Intramitochondrial accumulation of MIC19 is reduced.

subunits were also hindered, as there was a decline in the amount of dND3 and dND6 that had been incorporated into AIs (Fig. 9, D and E). Thus, disruption of the MICOS complex fully recapitulates the phenotype observed when the AIF-Mia40 translocation system is obstructed. Importantly, and in remarkable semblance to results obtained when dAIF is knocked down, CV AIs also accumulated in response to disruption of the MICOS complex (Fig. 9 F compared with Fig. 4 G). Combined with results from Fig. 8, we conclude that the AI phenotype observed when dAIF, dMia40, or dErv1 expression is disrupted is due to the compromised translocation

of dMia40 substrates, such as dMIC19, that are part of the MICOS complex.

Discussion

As *Drosophila* flight muscles are highly enriched with mitochondria and amenable to various genetic manipulations, we have studied dAIF function in *Drosophila* flight muscles and explored the consequences of mild, moderate, and severe dAIF dysfunction. We find that severely impairing dAIF function in *Drosophila* flight muscles produces adult flies that are essentially

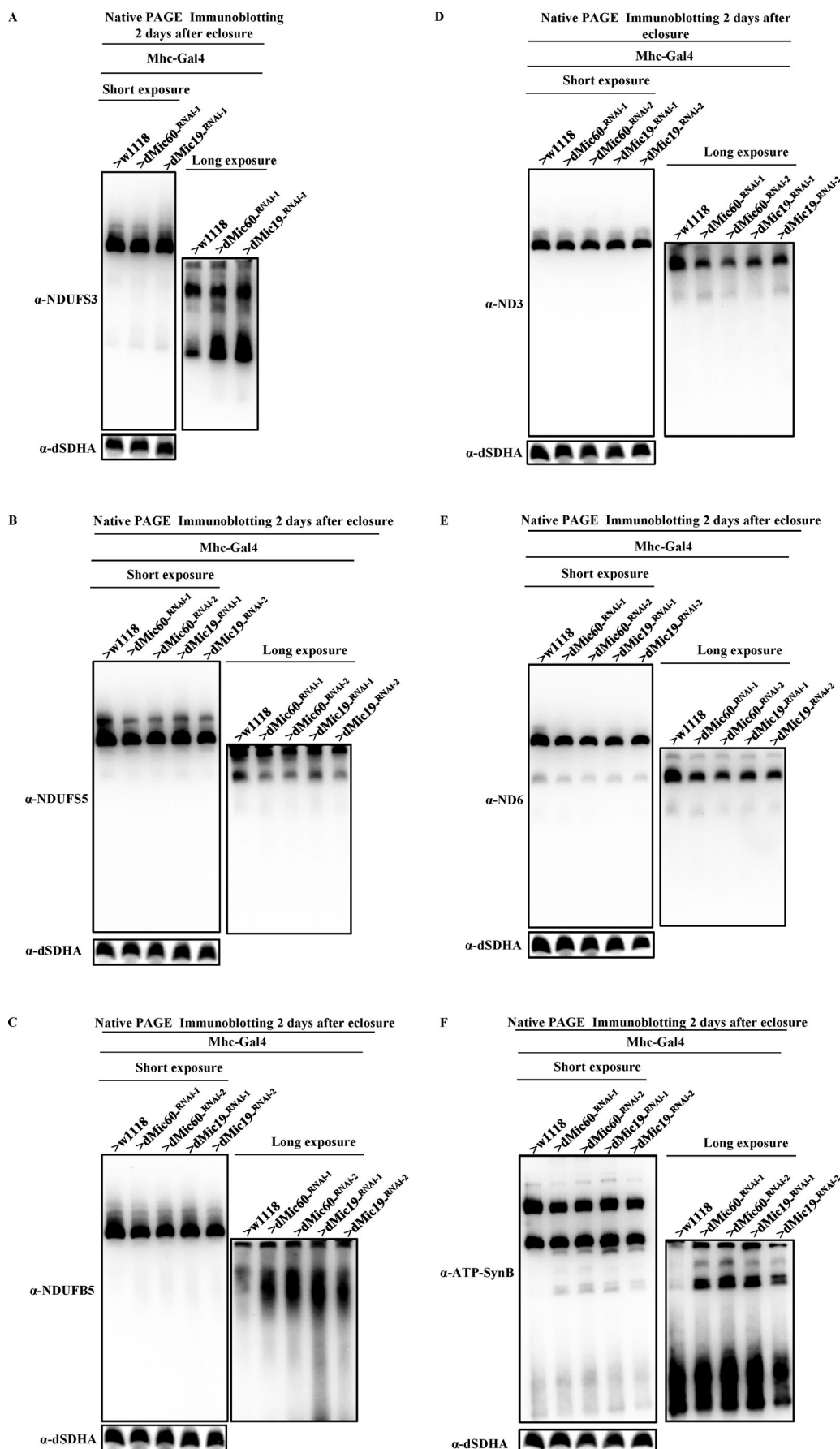


Figure 9. **The *Drosophila* orthologue of the Mia40 substrate CHCHD3/MIC19 regulates the biogenesis of AIs containing both nuclear- and mtDNA-encoded CI subunits. (A–F)** AI profile observed as a result of knocking down the expression of dMIC19 and dMIC60 with a transgenic RNAi construct. Mitochondrial preparations were obtained from flight muscles of flies with the genotypes listed and analyzed by BN-PAGE, followed by Western blotting with the antibodies shown.

paralyzed, have severe OXPHOS defects, and succumb to lethality within 3 d. However, a moderate disruption of dAIF impaired OXPHOS assembly while having relatively modest effects on locomotory ability. In classic hormesis fashion, and in agreement with the gene expression data from Fig. 2, the spontaneous activity of flies where dAIF was knocked down with the weakest Gal4 driver (mild disruption) was enhanced relative to wild-type controls (Owusu-Ansah, Song and Perri-mon, 2013; Ristow, 2014). Hence, we have a system that allows us to examine the extreme pathological consequences of dAIF dysfunction (when dAIF function is severely impaired), as well as the compensatory adaptive responses induced as a result of mild dAIF disruption.

We find that when the expression of dAIF, dMia40, or dErv1 is knocked down via transgenic RNAi expression, biogenesis of the P_p module stalls, resulting in a backlog and accumulation of the Q module. In addition, there is a robust accumulation of the P_D module. RNAi-mediated disruption of each of the four CI subunits that have been hypothesized to be transported by the Mia40-dependent disulfide relay system recapitulates a portion of the AI profile manifest when any of dAIF, dMia40, or dErv1 is genetically disrupted. Nevertheless, none recapitulated the full AI profile associated with loss of dAIF, dMia40, or dErv1. Significantly, the expression of dND3, dND4L, or dND6 was not decreased when any of the putative CI Mia40 substrates were genetically disrupted. Accordingly, we conclude that the CI AI profile apparent when dAIF, dMia40, or dErv1 expression is disrupted is not due to the compromised translocation of any one dMia40 CI substrate into the mitochondrion.

To account for the down-regulation of both nuclear- and mtDNA-encoded CI subunits that is evident when any of dAIF, dMia40, or dErv1 is knocked down, we searched for Mia40 substrates that are likely to affect multiple aspects of mitochondrial function. Typical Mia40 substrates contain twin cysteine-X₃-cysteine (CX₃C)₂ or twin cysteine-X₉-cysteine (CX₉C)₂ motifs and are <25 kD. A literature search identified CHCHD3/MIC19 as a Mia40 substrate that is part of the MICOS complex, and we confirmed that disruption of the AIF–Mia40–Erv1 complex impairs the intramitochondrial accumulation of dMIC19. RNAi-mediated knockdown of the *Drosophila* orthologue of dMIC19 recapitulates the CI AI distribution pattern that is detected when dAIF, dMia40, or dErv1 expression is disrupted. Similar results were obtained when the *Drosophila* orthologue of MIC60 (dMIC60) is knocked down. Accordingly, we conclude that dMIC19 is a Mia40 substrate that accounts for the CI AI profile observed when the expression of dAIF, dMia40, or dErv1 is disrupted.

In humans, genetic disruption of the *AIFM1* gene is known to cause an X-linked mitochondrial disorder. While the complete functional and biochemical consequences of various disease-causing mutations in AIF are still being explored, the cardinal

clinical features of AIF dysfunction typically include some form of muscular atrophy and neurodegeneration. Mouse models have proven instrumental in uncovering some of the molecular etiologies associated with various pathological mutations in AIF. However, modeling AIF dysfunction in *Drosophila* will make it possible to exploit the facile genetics of this organism to expand our knowledge of the role of AIF in bioenergetics.

In spite of the fact that no nuclear-encoded direct regulator of CV assembly has been identified as a Mia40 substrate, dAIF disruption alters the CV AI profile. This can be explained by our observation that disruption of the Mia40 substrate MIC19 impairs the assembly of CV. Moreover, there is a growing list of “non-canonical” Mia40 substrates that do not possess the characteristic (CX₃C)₂ or (CX₉C)₂ motifs and are >25 kD. A classic example is Ccs1, a copper chaperone for the yeast copper-zinc superoxide dismutase that has a CX₂CX₆CX₃₆CX_nC motif and is 27 kD (Reddehase et al., 2009). Our work does not exclude the possibility that additional canonical and noncanonical Mia40 substrates that regulate OXPHOS assembly may help account for the overall OXPHOS AI profiles produced when dAIF expression is impaired.

In conclusion, we have used *Drosophila* genetics and 21 novel antibodies to mechanistically track the “building blocks” (i.e., AIs) of CI when AIF is disrupted in vivo. An emerging theme in AIF biomedical research is the need to elucidate the molecular underpinnings of the extreme variability in phenotypes associated with various pathological AIF mutations. Many of the pathological mutations in AIF are localized to the NADH and flavin adenine dinucleotide-binding motifs. Because of the extensive homology in the NADH and flavin adenine dinucleotide-binding motifs of human and *Drosophila* AIF, specific AIF point mutations that are clinically relevant can be modeled in *Drosophila* and studied. We anticipate that future studies modeling some of these mutations in *Drosophila* should help unravel additional mechanisms by which AIF regulates cellular physiology. Going forward, we anticipate that the 21 antibodies we have generated, in particular the seven antibodies targeting all seven mtDNA-encoded CI subunits, will be instrumental in defining additional mechanisms by which CI assembly is regulated.

Materials and methods

Drosophila strains and genetics

Drosophila stocks were reared on standard cornmeal/molasses medium at 25°C. The transgenic Gal4 lines used were *y w*; *Dmef2-Gal4* (Ranganayakulu et al., 1996), *w*; *Mhc-Gal4* (Schuster et al., 1996), *Mhc-Gal4/SM6b* (Bloomington *Drosophila* Stock Center [BDSC]), and *Ubi-Gal4* (BDSC). The *tub-Gal80^{ts}* line used was from the BDSC.

Transgenic RNAi stocks for disrupting mRpS29/CG3633 (HMS02631), mRpS21/CG32854 (HMJ22164), mRpS16/CG8338 (HMJ30292), mRpS5/CG40049 (GL00562), mRpL20/CG11258

(HMJ22045), mRpL14/CG14048 (HMJ23590), dMia40/CG7950 (HMJ30199), dErv1/CG12534 (HMC03697), dMIC19/CG1715 (HMS01900), dMIC19/CG1715 (HMC02376), dMIC60/CG6455 (HMJ30307), dNDUFA8/CG3683 (GLC01699), dNDUFB7/CG5548 (HM05255), dNDUFB10/CG8844 (JF03271), dNDUFS5/CG11455 (HMC03861), dNDUFS2/CG1970 (HM05059), dNDUFV1/CG9140 (HMS01590), and dNDUFA12/CG3214 (HMS01584) were from the BDSC.

Transgenic RNAi stocks for disrupting dNDUFC2/CG12400 (KK112088), dNDUFA6/CG7712 (KK108758), and dAIF/CG7263 (GD822) were from the Vienna Drosophila Resource Center.

Transgenic stocks from the National Institute of Genetics (Japan) Drosophila Stock Center were dNDUFS6/CG8680 (8680R-3), dNDUFS7/CG9172 (9172R-2), dNDUFA11/CG9350 (9350R-2), dMIC60/CG6455 (6455R-2), and dAIF/CG7263 (2LG-0618).

Flies were generally housed in vials containing agar, molasses, yeast, and cornmeal medium supplemented with propionic acid and methylparaben at 25°C, except for the experiments involving Gal80, where they were raised at 18°C and shifted to 27°C at the appropriate time points.

Sequences for transgenic RNAi constructs

All sequences are listed 5' to 3' and are based on information associated with the transgenic constructs as listed on the websites of the respective *Drosophila* stock centers.

The short hairpin RNA constructs were HMS02631 (CCGCTG GACAGTGCAGTAA), HMJ22164 (CCGCACCGTTCTGGTGCA AAA), HMJ30292 (AACCGGAGGACAGCTGCTGAA), GL00562 (ATCAAGCTTGTAGCAGAAATA), HMJ22045 (CTCCGATATTCT GCTCAACAA), HMJ23590 (ATCCTGAAAACAGTTAGACAA), HM J30199 (TAGGTGGGAGTACATAAGATA), HMC03697 (CACAAC CGAGTGAACGACAAA), HMS01900 (CAGCAGCTAGAGGAACTT CAA), HMC02376 (TCCGACGATGTGGTCAAGCGA), HMJ30307 (CTGGACACCTACGATATCCTA), GLC01699 (CGACAAGTGTAT CAAAGATAA), HMC03861 (ACGCTACAAGCAGTGGCTCAA), HM S01590 (CTGGATCGTTAACGAGATCAA), and HMS01584 (AAG AAGCAGTAGTGTGGCATA).

The long hairpin RNAi constructs are listed below.

HM05255: GGGGCGAGGAAGAAGAAGAACTTTGACAGCTGCG GCGCAACCGAAATCTAAGAAAAACAATTTACGATGGGCA ACGCGCTGACGCACTACATGAAACCGGACGTGATGCCCGGCC CGGACGTGGTGGCCACCTTTGACCCACTGCTGGGCTTCAAGT CGCGCAAGGAGCGTGTGATGATCGCCACCCAGGAGGAGATGG AGTCCGCCAAGCTGCCGCTGGAATTCGCGACTAC.

JF03271: ACCCATAACTTGGTTCCGTGAGAGCATTGTGGAGCC GAACCAGCAGAAGCAGAATTGGTACCACCGCGCTTCCGCCG CGTTCCGACGATCGACCACTGCTACACGACGATGCCGTCTG CCGTTTTCGAGGCCGATCAGCAGTTCCGCCGGGATCGCATGGT CGACAACGAGATTGTCAACATTCTGCGCCAGCGCTTCGAGGACTG CACCCTCTACGAGGACCCGATCAGATGGTCAAGTGCAGGCCGCTG ATGGATCAGTACGAGAAGGCCACCGAGAAGTGGTTCATCAAGTA TGGCGACTTGGGAGGCTACGCCAATGCCAAGACCGCGTACAT GAAGCAGAAGCATCGTCTGATCTGGGAGCGTCTGATGAGACC AGTGGGACGTGGCATGAAGGAGGAGGCCGCCATTAACCTCC GCTTTT.

HM05059: GGACGAAGTGGAGGATGTGTTAACTACAAATCG AATCTGGGTGCAGCGGACCGAGGACATTGGGATCGTAACTGC

AGAAGAAGCTTTGAACTATGGCTTCAGTGGAGTTATGTTGCG TGGATCTGGCATAAAATGGGATCTTCGAAAAGCAGCAGCCGTA CGATGCCTATAATTTGGTAAACTTTGATGTTCCCATCGGCAC CAAAGGGGACTGCTACGACCGATATCTTTGCCGGGTCGAGGA AATGCGCCAGTCATTACGAATTATTGATCAATGCCTAAACCA AATGCCTGCTGGAGAAAATTAACCGGATGATGCCAAGGTGGC GCCTCCGTACCGGTCCGAAATGAAGACATCCATGGAGGCACT TATTCACCACTTCAAGTTATTTACCCAAGGATATCAAGTTCC ACCCGGGGCAACATACACGGCAATAGAGGCTCCGAAGGGCGA GTTTGGAGTTTACCTTATATCAGATGGGTCCAGTCTGTCATA CCGGTGCAAAATCAAAGCTCCAGGGTTTGCTCACTTGGCAGC TTTAGAGAAGATTGGAAGCAGCACATGCTAG.

KK112088: GAAGCCCGAGTTGATGAAAATGGCCGCGCCAC GCCGGCCACACCGCAGGCAATCGGATTCCATATCGGCGAGAG GAAAGAAGGCTCGTGGGTGCCCTTGTTCGTCAAAAAGTTCCAG CGGATCGTTCACGGCACTCATGTTGAT.

KK108758: TTGTACAGATTGAGGGCAGCCTTACGGGCTCC TCGCGTCCACGGACAGGATGGGGCGCACCTGCTGTACGGCT CGCTTACGGCTTACGTCGGGCCATTTGATTTGTTTTTATT TCTTTCTGTTTTCTACGACCAAATTGCTCCAAGCAGAACA GTGTGACCGCAGT.

GD822: GTCATCCCCAACGCCAGCATTGCTCGGCAGTTCCG GATGAAACCAATCTAAAGTTGGAGTTAAACAATGGAATGACT TTGATGTGCGACGTGGTGGTGGTCTGCGTGGGTTGCACGCCA AACACGGATCTCGCGGGACCCAGCAGGCTAGAGGTGGACAGA AGTCTCGGCGGTTTTGTGGTTAATGCAGAGCTGGAGGCCAGG CGGAACCTGTACGTGGCGGTGATGCTTCTGCTTCTTTCGAT CCTCTGCTGGGCGAGCGACGGGTGGAGCACCATGATCACTCG GTGCTCTGCTGGTGGCTGGC.

8680R-3: TGGCCAGCAAGCAATTGGTAAACAATTTGTCCAA CTCGGCCTTCCGCGACAGAATTGGATGTCCCCACTGGCCAGCG TTCGCCACTNCAAGCTGCCGCGGACATCGAGAAGGTCACA CACACCGGACAAGTGTTCGATAAAGGANGGACTACCGCAATGC CCGGTTCTGTAACGCCAAGCGGTATGTGAACGAGAAGTGGGG CATCAAGCTCATCGAGGAGGTGCCACCCAAGGAGTGCACCGA ACGAGTTGTCTTCTGCGACGGCGGCGATGGTCTTTGGGTCA TCCCAAGGTGTACATCAACCTGGACAAAACCCGGAATCACAT CTGCGGCTATCTGCGGCTGCGCTTCTGTCAGAAAAGATGACC.

9172R-2: ATGCTGCGTTCGGCGATGATGTATCGACCCTGTC CCGGGCTCTCCAAAGGCGATCTCAGACACCGAATGCGTCGAT TTCGGCGCTGCCCGCTCTGAATTTTGGCCCTGGTGGCGCAAC AACAAACGCTTCCAGTTGCCGAAGTGGCCCAAAATCTGCCCA AGAAGGGCTACTGCTCCGTTCCGGCACCAACAGTCTCTCGTT GCGGAGTGGTCACTGGCCAGACTGGACGATCTGCTCAACTGG GGTGCGAAGGGCTCGATCTGGCCACTGACTTTCCGTTTGGCC TGCTGTGCCGTCGAAATGATGCACATCGCTGCTCCGCGTTAC GACATGGATCGATATGGTGTGTGTTCGTGCTCTCCACGG TCAGGCCGATGTATCATCGTCTGCTGGCAGCTGACCAACAA AATGGCACCGGCCCTGCGAAAGNCTACGACCAAATGCCCGA GCCACGTTGGGTCTCTCCATGGGCAGC.

9350R-2: TGTGCTGCTCCGTTTCAAATACTACGACCATCCC GATGGCGAGGATGCCTTTGGCAAGATCGTGGCCACCAACA AGTACGCGGTATCCNCCGGCGTGGCTGGTCCATGTTTCGACG TCCTGACGCTCTCAAAGCCGCAAGGATATCTGCCACACTGG GCCGNTTTCGCCNTACAACACGGGTCCGCTGATGGGCATGNN CACGGCGTTCACTCTGACCACCTGGTGGCCACAAATNG CGCGCGCAAGGACGATAAAATCAACTACCTGATCGGCG

GTTCGCGGCTGGCGGCGTCTTTGGAGCCTGGAAACACA
ACCACGTAGCTGGTCTGTGCGCGGCTCTTCTGGGCATCG
CTGGTGTCAACAAGATGTCCATTGAACAGGGCTGGG
AGTTCTTCCCAACACACCGATCAAGCAGTATGGTGGTC
TGAACATTGCCGGAACGACTGGACCATTATGGCCGATC
CTCCCAAGAACTGGACCACGGAATA.

6455R-2: NTGTATCGGCTAGCGGTGNGAGATCAGTGCAAG
TGCGCCCTGCAGCGtNCNCNNCAGNAGACGACGCAACAAC
AGGCAATTGCGCGGAAGCAGCAGCGGTAAAGTGGCGGCGGGA
CCAGGGCAGGCGGCGAGGAGGAGCAGGGACAGCAAGGCGA
TCAAGGATATCAAGGATACCAGAGCCTGCCANCCGCATATGC
GCGAAGCTGTGCTTCGGCAAAGTGGTCTCTTCGTCTACCA
CTGGCAGCTGTGCGCGGTGTATCACCTACGCCAAATACGAC
GACGACTTCCGCAAATTGGTGGAGAAGAATGTACCGGCGCA
GGATCCGTATCAAGGTGGCTGTGAGGAGGAACCGCCATTC
AAGGGCATCAACAAGAAGCTCAACGATCAGATCGATAAGGTC
AAGTCTGGCATCGAGACAGTGACGTCCACGGTGGACTCGTTACA
TCTAAGGTGACGGGCTGTTTGGCGGCGGAGCGGCGAATGA
CAAGTCCAA.

Sequence for transgenic gRNA construct

dAIF/CG7263 (2LG-0618): GTCCGGCTAACAAGGCAGCCA.

Locomotor activity

Locomotor activity was assessed in two different ways.

Climbing ability assay: 20 adult male flies were placed in vials containing fly food. Subsequently, the vials were tapped gently to allow flies to settle at the bottom. The number of flies that climbed beyond the midpoint of the vial within 15 s were noted and recorded. This was repeated for 80 more flies (4 sets of 20). The number of flies that climbed beyond the midpoint of the vial were pooled together to obtain the number of flies that climbed beyond the midpoint of the vial per 100 flies. The whole experiment was repeated two more times to obtain three biological replicates, representing a total of 300 flies.

Spontaneous physical activity assay: Eight adult male flies were placed in a *Drosophila* activity monitor (TriKinetics). Movements were recorded continuously for at least 144 h on a 12-h/12-h dark/light cycle.

Lifespan analyses

Flies were collected and reared at a density of 25 male flies per vial in a Forma environmental chamber (ThermoFisher Scientific) at 25°C. Flies were scored for viability every day and transferred to vials containing fresh food every 2 d.

Survival analyses on a 5% sucrose diet

Male flies were collected and reared at a density of 25 flies per vial in vials containing 5% sucrose and 1% agar in PBS in a Forma environmental chamber (ThermoFisher Scientific) at 25°C. The percentage of flies that survived was assessed every day, with survivors transferred to fresh vials every 2 d.

Survival analyses on a high-fat diet

Male flies were collected and reared at a density of 25 flies per vial in vials containing 1% agar and 30% coconut oil in PBS in a Forma environmental chamber (ThermoFisher Scientific) at

25°C. The percentage of flies that survived was assessed every day, with survivors transferred to fresh vials every 2 d.

Starvation resistance assay

Male flies were collected and reared at a density of 25 flies per vial in vials containing 1% agar in PBS in a Forma environmental chamber (ThermoFisher Scientific) at 25°C. The percentage of flies that survived was assessed every day, with survivors transferred to fresh vials every 2 d.

Mitochondria purification

Mitochondrial purification was performed using a protocol described by [Rera et al. \(2011\)](#). Thoraxes were dissected and gently crushed with a dounce homogenizer in 500 µl of prechilled mitochondrial isolation buffer containing 0.25-M sucrose and 0.15-mM MgCl₂ supplemented with Halt protease inhibitors (Pierce) in 10-mM Tris-HCl, pH 7.4. Tissue homogenates were centrifuged twice at 500 *g* for 5 min at 4°C to remove insoluble material. Subsequently, the supernatant was recovered and centrifuged at 5,000 *g* for 5 min at 4°C. The pellet, which is enriched for mitochondria, was washed twice in the mitochondrial isolation buffer and stored at -80°C until further processing.

BN-PAGE

BN-PAGE was performed using NativePAGE gels from Life Technologies, following the manufacturer's instructions. Mitochondria were suspended in native PAGE sample buffer (Life Technologies) supplemented with digitonin and protease inhibitors and incubated on ice for 20 min. The digitonin:protein ratio used was 10:3. Following centrifugation at 20,000 *g* for 30 min, the supernatant was recovered, mixed with the G-250 sample additive (Life Technologies) and Native PAGE Sample Buffer (Life Technologies), and loaded onto 3–12% precast Bis-Tris Native PAGE gels (Life Technologies). The Native-Mark Protein standard (Life Technologies), run together with the samples, was used to estimate the molecular weight of the protein complexes. Electrophoreses was performed using the Native PAGE Running buffer (as anode buffer; Life Technologies) and the Native PAGE Running buffer containing 0.4% Coomassie G-250 (cathode buffer). Gels were stained with the Novex Colloidal Blue staining kit (Life Technologies) to reveal the protein complexes.

Silver staining

Silver staining of native gels was performed with the SilverXpress staining kit from Life Technologies, following the manufacturer's protocol.

In-gel CI, CIV, and CV activity

CI activity in native gels was performed by incubating the native gels in 0.1 mg/ml NADH, 2.5 mg/ml Nitroterazolium Blue Chloride, and 5-mM Tris-HCl (pH 7.4) at room temperature.

CIV activity in native gels was performed by incubating the native gels in 50-mM sodium phosphate (pH 7.2), 0.05% 3,3'-diaminobenzidine tetrahydrochloride, and 50-µM horse heart cytochrome C at room temperature.

CV activity in native gels was performed by preincubating the gel in 35-mM Tris-base and 0.27-M glycine (pH 8.4) for 3 h and then subsequently in 35-mM Tris-base, 0.27-M glycine (pH 8.4), 14-mM MgSO₄, 0.2% wt/vol Pb(NO₃)₂, and 8-mM ATP at room temperature.

Generation of peptide polyclonal antibodies

Rabbit peptide polyclonal antibodies recognizing various segments of specific target proteins in *Drosophila* were generated using the following synthetic peptides: NKYPNHQVCVTKPS, dAIF (CG7263); RVQKLDAEPSSKVTSK, dMIC19 (CG7263); RGTLPFRYDKLMY, dND1 (CG34092); SDNNLMSTEASLK, dND2 (CG34063); HEWNQGMNLWSN, dND3 (CG34076); QHGKLFSGVYSFSSGK, dND4 (CG34085); RTHGNDYFQSFSIM, dND4L (CG34086); DQGWSEYFGGQHLYQK, dND5 (CG34083); KLFKGPIRMMS, dND6 (CG34089); DGSSRPYRCKIKAPG, dNDUFS2 (CG1970); RKGQEFFADPPRVDAY, dNDUFS5 (CG11455); SKLGLP RQNWMSP, dNDUFS6 (CG8680); RPSVAKYHRISKE, dNDUFB5 (CG9762); SETGGVKPMVIAGRM, dNDUFB6 (CG13240); KQYPSPGVKHYTFEK, dNDUFB8 (CG3192); PEIEKRMQLHAKRVS, dNDUFB1 (CG9140); PNKVEAWEPKAKKQ Target, dNDUFA12 (CG3214); KRGYATCPRPVGDL, dUQCRC2 (CG4169); GLTSKWDYENKKWKN, dCOXIV (CG10664); NLGLQDSASPLMEQ, dMtCOXII (CG34069); and DNEVSTVPPAIRSY, dSDHA (CG17246).

Immunoblotting

For immunoblotting of samples in blue native gels, protein complexes from 3–12% precast Bis-Tris Native PAGE gels (Life Technologies) were transferred to polyvinylidene difluoride membranes (Bio-Rad). For immunoblotting of denatured samples in whole tissue lysates, thoraxes were homogenized in radioimmunoprecipitation assay buffer (150-mM NaCl, 1% Triton X-100, 0.5% sodium deoxycholate, 0.1% SDS, and 50-mM Tris-HCl, pH 8) supplemented with Halt protease inhibitors (Pierce), resolved on mini-PROTEAN TGX stain-free gels from Bio-Rad, and transferred to polyvinylidene difluoride membranes. In both instances (native and nonnative gels), the membrane was subsequently blocked in 5% (wt/vol) nonfat dry milk in TBS for 30 min and incubated in the appropriate primary antibody dissolved in 2% BSA and 0.1% Tween 20 in TBS (TBST) overnight at 4°C. Following the overnight incubation, the blot was rinsed four times for 10 min each in 0.1% TBST, blocked for 30 min in 5% (wt/vol) nonfat dry milk in TBST, and incubated for 2 h with the appropriate HRP-conjugated secondary antibody dissolved in 2% BSA and 0.1% TBST. After incubation in the secondary antibody, samples were rinsed four times for 10 min each in 0.1% TBST. Immunoreactivity was detected by ECL and analyzed by a ChemiDoc Gel imaging system from Bio-Rad. Primary antibodies used were anti-NDUFS3 (Abcam, ab14711), anti-ATPsynβ (Life Technologies, A-21351), anti-VDAC1/Porin (Abcam, ab14734), anti-cytochrome C (Abcam, ab13575), anti-Hsp60 (Cell Signaling Technology, 4869S), anti-Hsp90 (Cell Signaling Technology, 4874S), and the rabbit polyclonal antibodies generated by Biomatik. Secondary antibodies used were goat anti-rabbit HRP (Pierce, PI31460) and goat anti-mouse HRP (Pierce, PI31430). There are major discrepancies between the migration behavior of membrane and soluble protein

markers. Accordingly, estimating the sizes of membrane proteins such as OXPHOS complexes or AIs on blue native gels using standard soluble protein markers produces spurious results. Consequently, we chose not to estimate the sizes of proteins on blue native gels using standard protein markers. OXPHOS complexes and AIs were assessed based on their known constituent protein subunits.

Quantitative real-time RT-PCR

Total RNA was isolated from thoraxes using TRIzol Reagent (Invitrogen) and, following the elimination of genomic DNA, reverse transcribed using the iScript cDNA Synthesis kit from Bio-Rad (catalog number 1708891). The PCR reaction was performed using Bio-Rad's iQ SYBR Green Supermix (catalog number 1708882). The following primer sequences, listed 5' to 3', were used: Hsp22F (TGGCTATAGCTCCAGGCACT) and Hsp22R (ACGCTCCTTGAGTGTCTCTCT); Hsp26F (TACAAGGTTCCCGATGGCTA) and Hsp26R (GGTCCCACTTGCTGAATTTG); Hsp70AaF (CGGAGTCTCCATTCCAGGTGT) and Hsp70AaR (GCTGACGTTCCAGGATTCCAT); Hsp70BaF (GGCTTTTACAGACTC GGAAC) and Hsp70BaR (CTTTGAAAGGCCAGTGCTTC); Jafrac1F (ACAAGGGCAAATACCTGGTG) and Jafrac1R (AAGTGGGTGAAC TGGCTGTC); CG12896F (GACGAGGAGCAGAAGAAGGA) and CG12896R (GGGAGTCAATGGTCTCTCAGA); Prx2540-2F (TTG ACTCCCTCCAGCTGACT) and Prx2540-2R (ACTCCAGACGGC ATGGATAC); GSTS1F (AAGTTGGTCACCCTGAATGC) and GSTS1R (GCGCTTGACCATGTAGTTCA); GSTD2F (TGGATTCTCGACACCTTCC) and GSTD2R (CCACCTGGAGACATTGGAGT); and GSTD6F (AACCCGGAACCTCAGGAGAAT) and GSTD6R (AAC CATTTCCGGTTGTGGAAA).

Statistics

Except where noted, P values are based on the Student's *t* test for unpaired two-tailed samples. The fold change shown refers to the mean ± SEM; *, *P* < 0.05; **, *P* < 0.01; ***, *P* < 0.001.

Online supplemental material

Fig. S1 provides additional evidence and a schematic showing that the synthesis of multiple AIs containing nuclear-encoded subunits is impaired when dAIF is disrupted. Fig. S2 depicts data from dAIF-s, dAIF-m, and dAIF-w flies showing that AIs containing both nuclear- and mitochondria-encoded subunits are impaired when dAIF is disrupted. Fig. S3 shows the kinetics of appearance of AIs when the Q, N, or P_p modules are disrupted. Fig. S4 gives further evidence that disrupting the production of the Q, N, or P_p modules does not always lead to a reduction in expression of dND3 and dND6.

Acknowledgments

We thank members of the Owusu-Ansah laboratory for general discussions and Michael Schlame (New York University, New York, NY), Barbara Corneo (Columbia University, New York, NY), Jeanine D'Armiento (Columbia University), Wes Grueber (Columbia University), Richard Kitsis (Albert Einstein College of Medicine, New York, NY), Andrew Marks (Columbia University), Martin Picard (Columbia University), and Mimi

Shirasu-Hiza (Columbia University) for fly stocks, reagents, and critical discussions. We acknowledge the BDSC, the National Institute of Genetics (Japan), and the Vienna Drosophila Resource Center for various fly strains. We appreciate Sandra Jones's technical assistance in performing the physical activity assays using the trikinetics system.

Work in the Owusu-Ansah laboratory is supported by a Provost Junior Faculty grant to support Columbia's diversity efforts, an Irma T. Hirschl Trust award, and National Institutes of Health grants DK112074 (R21), AR077312 (R21), and GM124717 (R35).

The authors declare no competing financial interests.

Author contributions: E. Owusu-Ansah conceived the project, designed experiments, and supervised the work. A. Murari performed all the experiments described in Figs. 4–9, and N.S. Goparaju performed the experiments described in Fig. 2. A. Murari, S.-K. Rhooms, M. Villanueva, and E. Owusu-Ansah performed all other experiments, including setting up genetic crosses. E. Owusu-Ansah, A. Murari, S.-K. Rhooms, and N.S. Goparaju analyzed and discussed results. E. Owusu-Ansah wrote the manuscript and got feedback from A. Murari, S.-K. Rhooms, and N.S. Goparaju.

Submitted: 13 January 2020

Revised: 1 June 2020

Accepted: 26 June 2020

References

- Agip, A.A., J.N. Blaza, H.R. Bridges, C. Viscomi, S. Rawson, S.P. Muench, and J. Hirst. 2018. Cryo-EM structures of complex I from mouse heart mitochondria in two biochemically defined states. *Nat. Struct. Mol. Biol.* 25: 548–556. <https://doi.org/10.1038/s41594-018-0073-1>
- Ardissone, A., G. Piscosquito, A. Legati, T. Langella, E. Lamantea, B. Garavaglia, E. Salsano, L. Farina, I. Moroni, D. Pareyson, et al. 2015. A slowly progressive mitochondrial encephalomyopathy widens the spectrum of AIFM1 disorders. *Neurology*. 84:2193–2195. <https://doi.org/10.1212/WNL.0000000000001613>
- Arnoult, D., P. Parone, J.C. Martinou, B. Antonsson, J. Estaquier, and J.C. Ameisen. 2002. Mitochondrial release of apoptosis-inducing factor occurs downstream of cytochrome c release in response to several proapoptotic stimuli. *J. Cell Biol.* 159:923–929. <https://doi.org/10.1083/jcb.200207071>
- Berger, I., Z. Ben-Neriah, T. Dor-Wolman, A. Shaag, A. Saada, S. Zenvirt, A. Raas-Rothschild, M. Nadjari, K.H. Kaestner, and O. Elpeleg. 2011. Early prenatal ventriculomegaly due to an AIFM1 mutation identified by linkage analysis and whole exome sequencing. *Mol. Genet. Metab.* 104: 517–520. <https://doi.org/10.1016/j.ymgme.2011.09.020>
- Brand, A.H., and N. Perrimon. 1993. Targeted gene expression as a means of altering cell fates and generating dominant phenotypes. *Development*. 118:401–415.
- Cheung, E.C., N. Joza, N.A. Steenaart, K.A. McClellan, M. Neuspiel, S. McNamara, J.G. MacLaurin, P. Rippstein, D.S. Park, G.C. Shore, et al. 2006. Dissociating the dual roles of apoptosis-inducing factor in maintaining mitochondrial structure and apoptosis. *EMBO J.* 25: 4061–4073. <https://doi.org/10.1038/sj.emboj.7601276>
- Darshi, M., K.N. Trinh, A.N. Murphy, and S.S. Taylor. 2012. Targeting and import mechanism of coiled-coil helix coiled-coil domain-containing protein 3 (ChChd3) into the mitochondrial intermembrane space. *J. Biol. Chem.* 287:39480–39491. <https://doi.org/10.1074/jbc.M112.387696>
- Fiedorczuk, K., J.A. Letts, G. Degliesposti, K. Kaszuba, M. Skehel, and L.A. Sazanov. 2016. Atomic structure of the entire mammalian mitochondrial complex I. *Nature*. 538:406–410. <https://doi.org/10.1038/nature19794>
- Formosa, L.E., M.G. Dibley, D.A. Stroud, and M.T. Ryan. 2018. Building a complex complex: Assembly of mitochondrial respiratory chain complex I. *Semin. Cell Dev. Biol.* 76:154–162. <https://doi.org/10.1016/j.semcdb.2017.08.011>
- Garcia, C.J., J. Khajeh, E. Coulanges, E.I. Chen, and E. Owusu-Ansah. 2017. Regulation of Mitochondrial Complex I Biogenesis in Drosophila Flight Muscles. *Cell Rep.* 20:264–278. <https://doi.org/10.1016/j.celrep.2017.06.015>
- Ghezzi, D., I. Sevrioukova, F. Invernizzi, C. Lamperti, M. Mora, P. D'Adamo, F. Novara, O. Zuffardi, G. Uziel, and M. Zeviani. 2010. Severe X-linked mitochondrial encephalomyopathy associated with a mutation in apoptosis-inducing factor. *Am. J. Hum. Genet.* 86:639–649. <https://doi.org/10.1016/j.ajhg.2010.03.002>
- Guerrero-Castillo, S., F. Baertling, D. Kownatzki, H.J. Wessels, S. Arnold, U. Brandt, and L. Nijtmans. 2017. The Assembly Pathway of Mitochondrial Respiratory Chain Complex I. *Cell Metab.* 25:128–139. <https://doi.org/10.1016/j.cmet.2016.09.002>
- Hangen, E., O. Féraud, S. Lachkar, H. Mou, N. Doti, G.M. Fimia, N.V. Lam, C. Zhu, I. Godin, K. Muller, et al. 2015. Interaction between AIF and CHCHD4 Regulates Respiratory Chain Biogenesis. *Mol. Cell.* 58: 1001–1014. <https://doi.org/10.1016/j.molcel.2015.04.020>
- Hell, K. 2008. The Erv1-Mia40 disulfide relay system in the intermembrane space of mitochondria. *Biochim. Biophys. Acta.* 1783:601–609. <https://doi.org/10.1016/j.bbamcr.2007.12.005>
- Klein, J.A., C.M. Longo-Guess, M.P. Rossmann, K.L. Seburn, R.E. Hurd, W.N. Frankel, R.T. Bronson, and S.L. Ackerman. 2002. The harlequin mouse mutation downregulates apoptosis-inducing factor. *Nature*. 419: 367–374. <https://doi.org/10.1038/nature01034>
- McGuire, S.E., Z. Mao, and R.L. Davis. 2004. Spatiotemporal gene expression targeting with the TARGET and gene-switch systems in Drosophila. *Sci. STKE*. 2004:pl6.
- Meyer, K., S. Buettner, D. Ghezzi, M. Zeviani, D. Bano, and P. Nicotera. 2015. Loss of apoptosis-inducing factor critically affects MIA40 function. *Cell Death Dis.* 6: e1814. <https://doi.org/10.1038/cddis.2015.170>
- Modjtahedi, N., and G. Kroemer. 2016. CHCHD4 links AIF to the biogenesis of respiratory chain complex I. *Mol. Cell. Oncol.* 3: e1074332. <https://doi.org/10.1080/23723556.2015.1074332>
- Otera, H., S. Ohsakaya, Z. Nagaura, N. Ishihara, and K. Mihara. 2005. Export of mitochondrial AIF in response to proapoptotic stimuli depends on processing at the intermembrane space. *EMBO J.* 24:1375–1386. <https://doi.org/10.1038/sj.emboj.7600614>
- Owusu-Ansah, E., W. Song, and N. Perrimon. 2013. Muscle mitohormesis promotes longevity via systemic repression of insulin signaling. *Cell*. 155:699–712. <https://doi.org/10.1016/j.cell.2013.09.021>
- Ranganayakulu, G., R.A. Schulz, and E.N. Olson. 1996. Wingless signaling induces nautilus expression in the ventral mesoderm of the Drosophila embryo. *Dev. Biol.* 176:143–148. <https://doi.org/10.1006/dbio.1996.9987>
- Reddehase, S., B. Grumbt, W. Neupert, and K. Hell. 2009. The disulfide relay system of mitochondria is required for the biogenesis of mitochondrial Ccs1 and Sod1. *J. Mol. Biol.* 385:331–338. <https://doi.org/10.1016/j.jmb.2008.10.088>
- Rera, M., S. Bahadorani, J. Cho, C.L. Koehler, M. Ulgherait, J.H. Hur, W.S. Ansari, T. Lo, Jr., D.L. Jones, and D.W. Walker. 2011. Modulation of longevity and tissue homeostasis by the Drosophila PGC-1 homolog. *Cell Metab.* 14(5):623–634. <https://doi.org/10.1016/j.cmet.2011.09.013>
- Rhooms, S.K., A. Murari, N.S.V. Goparaju, M. Villanueva, and E. Owusu-Ansah. 2019. Insights from Drosophila on mitochondrial complex I. *Cell. Mol. Life Sci.* 77:607–618. <https://doi.org/10.1007/s00018-019-03293-0>
- Rinaldi, C., C. Grunseich, I.F. Sevrioukova, A. Schindler, I. Horkayne-Szakaly, C. Lamperti, G. Landouré, M.L. Kennerson, B.G. Burnett, C. Bönnemann, et al. 2012. Cowchock syndrome is associated with a mutation in apoptosis-inducing factor. *Am. J. Hum. Genet.* 91:1095–1102. <https://doi.org/10.1016/j.ajhg.2012.10.008>
- Ristow, M. 2014. Unraveling the truth about antioxidants: mitohormesis explains ROS-induced health benefits. *Nat. Med.* 20:709–711. <https://doi.org/10.1038/nm.3624>
- Sakowska, P., D.C. Jans, K. Mohanraj, D. Riedel, S. Jakobs, and A. Chacinska. 2015. The Oxidation Status of Mic19 Regulates MICOS Assembly. *Mol. Cell. Biol.* 35:4222–4237. <https://doi.org/10.1128/MCB.00578-15>
- Schuster, C.M., G.W. Davis, R.D. Fetter, and C.S. Goodman. 1996. Genetic dissection of structural and functional components of synaptic plasticity. I. Fasciclin II controls synaptic stabilization and growth. *Neuron*. 17:641–654. [https://doi.org/10.1016/S0896-6273\(00\)80197-X](https://doi.org/10.1016/S0896-6273(00)80197-X)
- Stroud, D.A., E.E. Surgenor, L.E. Formosa, B. Reljic, A.E. Frazier, M.G. Dibley, L.D. Osellame, T. Stait, T.H. Beilharz, D.R. Thorburn, et al. 2016. Accessory subunits are integral for assembly and function of human mitochondrial complex I. *Nature*. 538:123–126. <https://doi.org/10.1038/nature19754>

- Susin, S.A., H.K. Lorenzo, N. Zamzami, I. Marzo, B.E. Snow, G.M. Brothers, J. Mangion, E. Jacotot, P. Costantini, M. Loeffler, et al. 1999. Molecular characterization of mitochondrial apoptosis-inducing factor. *Nature*. 397:441–446. <https://doi.org/10.1038/17135>
- Troulinaki, K., S. Büttner, A. Marsal, S. Maida, K. Meyer, F. Bertan, A. Gioran, A. Piazzesi, A. Fornarelli, P. Nicotera, et al. 2018. WAH-1/AIF regulates mitochondrial oxidative phosphorylation in the nematode *Caenorhabditis elegans*. *Cell Death Discov.* 4:2. <https://doi.org/10.1038/s41420-017-0005-6>
- Vahsen, N., C. Candé, J.J. Brière, P. Bénit, N. Joza, N. Larochette, P.G. Massaro, M.O. Pequignot, N. Casares, V. Lazar, et al. 2004. AIF deficiency compromises oxidative phosphorylation. *EMBO J.* 23: 4679–4689. <https://doi.org/10.1038/sj.emboj.7600461>
- Wischhof, L., A. Gioran, D. Sonntag-Bensch, A. Piazzesi, M. Stork, P. Nicotera, and D. Bano. 2018. A disease-associated Aifm1 variant induces severe myopathy in knockin mice. *Mol. Metab.* 13:10–23. <https://doi.org/10.1016/j.molmet.2018.05.002>
- Yu, S.W., H. Wang, M.F. Poitras, C. Coombs, W.J. Bowers, H.J. Federoff, G.G. Poirier, T.M. Dawson, and V.L. Dawson. 2002. Mediation of poly(ADP-ribose) polymerase-1-dependent cell death by apoptosis-inducing factor. *Science*. 297:259–263. <https://doi.org/10.1126/science.1072221>
- Yu, S.W., Y. Wang, D.S. Frydenlund, O.P. Ottersen, V.L. Dawson, and T.M. Dawson. 2009. Outer mitochondrial membrane localization of apoptosis-inducing factor: mechanistic implications for release. *ASN Neuro.* 1: e00021. <https://doi.org/10.1042/AN20090046>

Supplemental material

Q module

↓

Q + Pp module

↓

Q + P module
(Q + Pp + P_D module)

[illegible]

Murari et al.
AIF's role in complex I biogenesis

Native PAGE Immunoblotting 2 days after eclosure

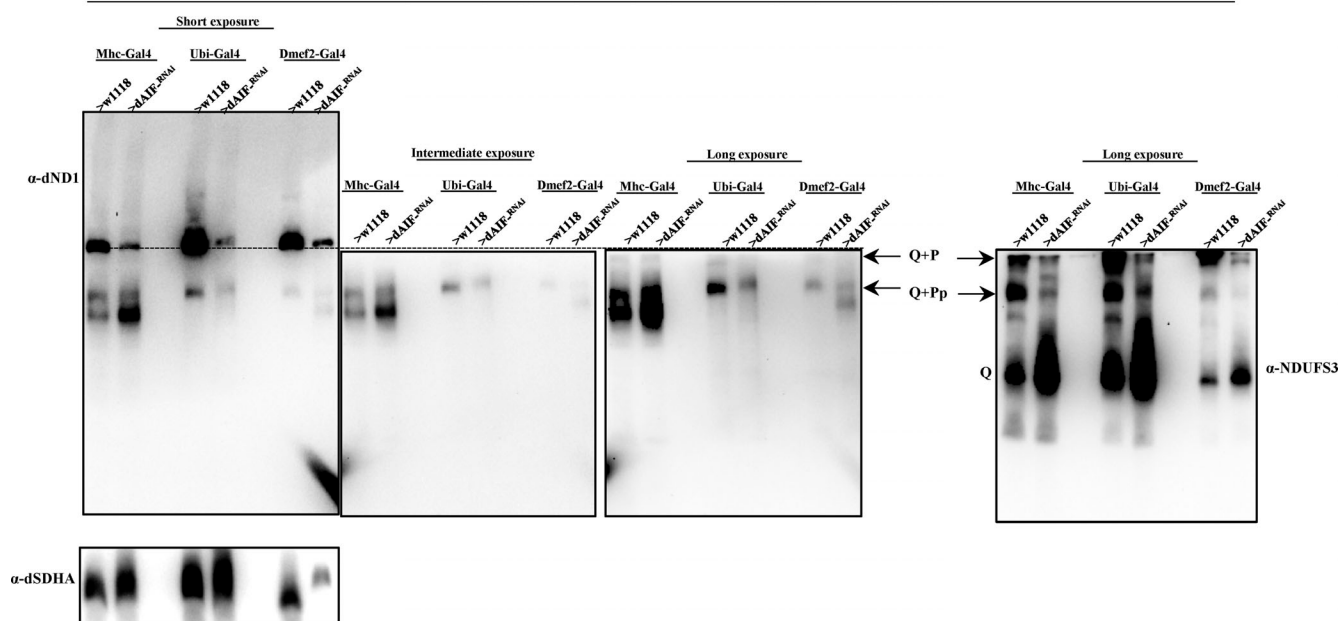


Figure S2. **Als containing both nuclear- and mitochondria-encoded subunits are impaired when dAIF is disrupted.** Mitochondrial preparations from flight muscles isolated from adult flies with the genotypes shown 2 d after eclosure were analyzed by BN-PAGE, followed by immunoblotting with the indicated antibodies. The blots were imaged following a short, intermediate, and long exposure to detect both the holoenzymes and Als produced when the different Gal4 lines were used. The antibodies used were anti-dND1 (left panel) and anti-NDUFS3, which detects dNDUFS3 (right panel). Anti-dSDHA was used as a loading control. Note that the far-right panel is the same as the far-right panel in Fig. S1 B.

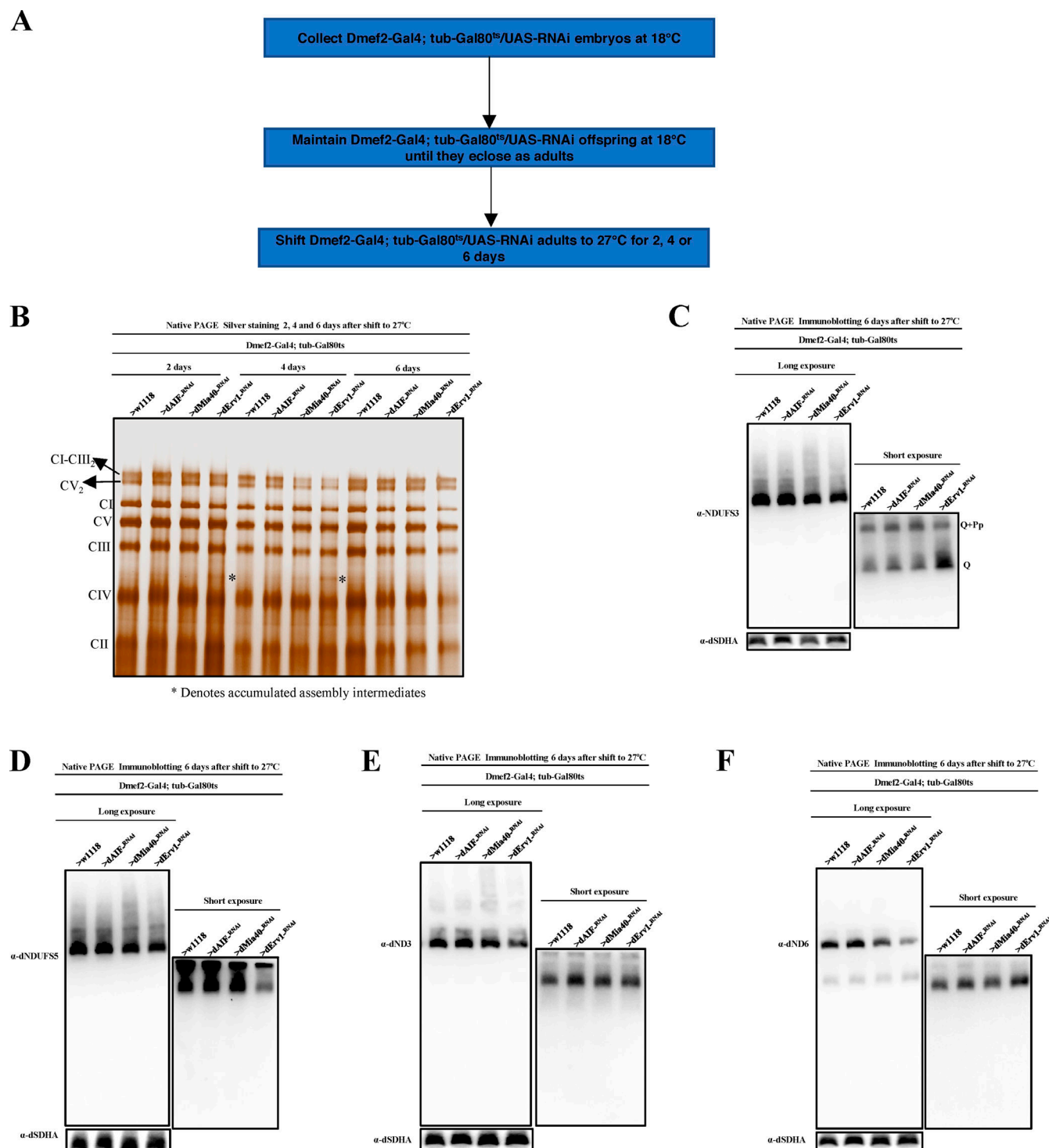


Figure S3. The kinetics of appearance of AIs when the Q, N, or P_p modules are disrupted. (A) The tub-Gal80^{ts} transgene expresses a temperature-sensitive version of Gal80, which is active at 18°C but inactive at 27°C, under the control of a tubulin promoter. Gal80 inhibits Gal4 activity. Accordingly, embryos expressing Dmef2-Gal4, tub-Gal80^{ts}, and the indicated UAS-RNAi transgenes were raised at 18°C (to prevent Gal4 activity) until they eclosed as adults. Subsequently, the flies were shifted to 27°C for 2, 4, or 6 d to allow the RNAi constructs to be expressed as a result of the relief of Gal4 inhibition by Gal80. **(B)** Mitochondrial preparations from flight muscles isolated from adult flies with the genotypes shown 2, 4, or 6 d after shifting to 27°C were analyzed by silver staining of native gels. **(C–F)** Mitochondrial preparations from flight muscles isolated from adult flies with the genotypes shown 6 d after shifting to 27°C were analyzed by BN-PAGE, followed by immunoblotting with the antibodies shown. The antibodies used were anti-NDUF53, which detects dNDUF53 (C), anti-dNDUF55 (D), anti-dND3 (E), and anti-dND6 (F). Anti-dSDHA was used as a loading control.

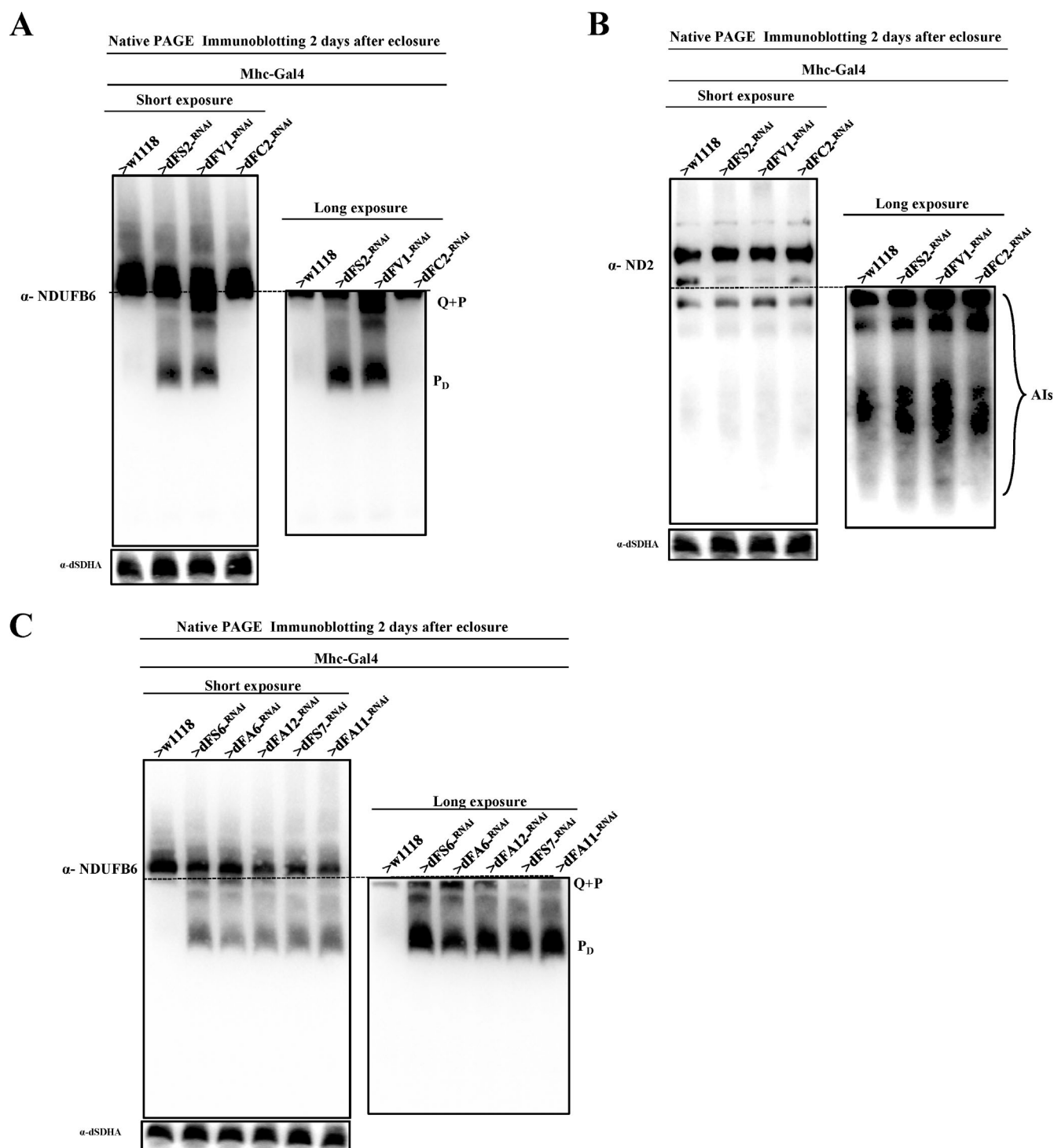


Figure S4. **Disrupting the production of the Q, N, or P_D modules does not inevitably lead to a reduction in expression of dND3 and dND6. (A–C)** Mitochondrial preparations from flight muscles isolated from adult flies with the genotypes shown 2 d after eclosure were analyzed by BN-PAGE, followed by immunoblotting with the antibodies shown. The antibodies used were anti-dNDUFB6 (A), anti-dND2 (B), and anti-dNDUFB6 (C). Anti-dSDHA was used as a loading control.